

Causal Invariance Learning via Efficient Optimization of a Nonconvex Objective

Zhenyu Wang^{1,*}, Yifan Hu^{2,3,*}, Peter Bühlmann^{4,†}, and Zijian Guo^{1,†}

¹Department of Statistics, Rutgers University, USA

²College of Management of Technology, EPFL, Switzerland

³Department of Computer Science, ETH Zürich, Switzerland

⁴Seminar for Statistics, ETH Zürich, Switzerland

December 18, 2024

Abstract

Data from multiple environments offer valuable opportunities to uncover causal relationships among variables. Leveraging the assumption that the causal outcome model remains invariant across heterogeneous environments, state-of-the-art methods attempt to identify causal outcome models by learning invariant prediction models and rely on exhaustive searches over all (exponentially many) covariate subsets. These approaches present two major challenges: 1) determining the conditions under which the invariant prediction model aligns with the causal outcome model, and 2) devising computationally efficient causal discovery algorithms that scale polynomially, instead of exponentially, with the number of covariates. To address both challenges, we focus on the additive intervention regime and propose nearly necessary and sufficient conditions for ensuring that the invariant prediction model matches the causal outcome model. Exploiting the essentially necessary identifiability conditions, we introduce Negative Weight Distributionally Robust Optimization (NegDRO), a nonconvex continuous minimax optimization whose global optimizer recovers the causal outcome model. Unlike standard group DRO problems that maximize over the simplex, NegDRO allows negative weights on environment losses, which break the convexity. Despite its nonconvexity, we demonstrate that a standard gradient method converges to the causal outcome model, and we establish the convergence rate with respect to the sample size and the number of iterations. Our algorithm avoids exhaustive search, making it scalable especially when the number of covariates is large. The numerical results further validate the efficiency of the proposed method.

1 Introduction

Establishing causal relationships between an outcome and multiple covariates is a fundamental objective in various fields, including education [Nye et al., 2000], economics [Duflo et al., 2007, Ludwig et al., 2013], epidemiology [Baicker et al., 2013], and computer science [Schölkopf et al., 2021, Schölkopf, 2022, Farrell et al., 2018, Sharma and Kiciman, 2020]. In many cases, the causal structure is unknown: some covariates may affect the outcome, others may be affected by the outcome, some are confounded with a hidden variable, and some may have no causal connection at all. In such settings, statistical learning approaches that focus on minimizing training errors tend to capture correlations present in the data, but fail to disentangle true

* These authors contributed equally to this work. † Correspondence should be addressed to these authors.

causal relationships. This limitation highlights the need for methods capable of learning not just predictive models, but also the underlying causal structure, identifying causal variables, and estimating their effects.

A thought experiment from [Beery et al. \[2018\]](#) illustrates the advantage of a causal model compared to a standard prediction model trained to minimize the training error. Consider the task of classifying images of cows and camels, where cows are predominantly photographed in green pastures and camels in brown deserts. Let X_1 represent the animal’s shape and X_2 represent the background color, with the outcome label $Y \in \{\text{cow}, \text{camel}\}$. A standard model trained to minimize training error would rely on X_2 (background color) for the predictions, leading to errors when cows appear on brown beaches. This scenario underscores the importance of distinguishing causal features like X_1 (animal’s shape) from spurious correlations such as X_2 (background color). This process - separating the true causes of the outcome from non-causal features and estimating their effects - is referred to as causal discovery.

The availability of heterogeneous multi-environment data enables causal discovery by learning the invariant prediction model across multiple environments [[Peters et al., 2016](#), [Meinshausen et al., 2016](#), [Ghasami et al., 2017](#), [Pfister et al., 2019, 2021](#), [Fan et al., 2023](#)]. We illustrate the main idea of the invariant prediction model by considering a specific scenario of the thought experiment: in one dataset, cows are commonly photographed in green pastures, while in another dataset, cows appear in both brown beaches and green pastures. By leveraging such heterogeneous datasets collected from two distinct environments, we tell that the animal’s shape X_1 maintains an invariant relationship with the outcome label Y , whereas the background color X_2 has a changing association with the outcome label across environments. In addition to identifying the causal effect, invariant prediction models enhance generalization to unseen populations that may exhibit distributional shifts from the observed environments. This robustness has been demonstrated across a range of studies, highlighting the practical advantages of (nearly) invariant prediction models for out-of-distribution performance [[Rojas-Carulla et al., 2018](#), [Magliacane et al., 2018](#), [Arjovsky et al., 2019](#), [Wang et al., 2022](#)].

Despite the success of learning invariant prediction models across environments, there is a lack of understanding of the following two fundamental questions,

(Q1) When does the invariant prediction model successfully recover the true causal outcome model?

(Q2) How can we design computationally efficient algorithms to learn the invariant prediction model?

In this paper, we address both questions within the additive intervention regime introduced in Section 3.1. For **(Q1)**, we establish nearly necessary and sufficient conditions that delineate when the invariant prediction model achieves the *causal identification*, i.e., when the invariant prediction model finds the true causal relationship. For **(Q2)**, we propose a novel nonconvex continuous minimax optimization framework for learning invariant prediction models. Despite the inherent nonconvexity, we design a computationally efficient algorithm that provably converges to global optimality, which corresponds to the causal outcome model. In particular, our algorithm scales polynomially with the dimension of the covariates.

1.1 Problem Formulations and Gaps

We introduce here the setup of causal invariance learning with data collected from multiple environments. Particularly, we consider multiple environments denoted as $\mathcal{E} = \{1, 2, \dots, |\mathcal{E}|\}$. For each environment $e \in \mathcal{E}$, we observe n_e i.i.d samples $\{x_i^{(e)}, y_i^{(e)}\}_{i=1}^{n_e}$ drawn from the distribution of $(X^{(e)}, Y^{(e)})$, where $X^{(e)} \in \mathbb{R}^p$ and $Y^{(e)} \in \mathbb{R}$ represent the covariates and the outcome for the e -th environment, respectively. We use $X_{S^*}^{(e)}$ with $S^* \subseteq [p]$ to denote the true observed causal variables for the outcome $Y^{(e)}$. The essential assumptions of causal invariance learning go as follows: the causal outcome model from $X_{S^*}^{(e)}$ to $Y^{(e)}$ remains invariant while the marginal distributions of $X^{(e)}$ vary across environments $e \in \mathcal{E}$. The goal of causal invariance

learning is to identify the causal covariates $X_{S^*}^{(e)}$ and estimate the causal effect, provided the data samples $\{x_i^{(e)}, y_i^{(e)}\}_{i=1}^{n_e}$. We note that the setting allows for hidden confounding variables.

Next, we briefly review the existing literature on causal invariance learning, focusing on the gaps in answering **(Q1)** and **(Q2)**, while other related literature will be discussed in Section 1.3. Regarding the causal identification question **(Q1)**, prior works such as Fan et al. [2023] and Yin et al. [2024] impose abstract identification conditions, requiring the multiple environments to exhibit sufficient heterogeneity, in the sense that, if a subset of variables includes non-direct causes of the outcome, it fails to provide invariant prediction models across the observed environments. However, these works do not provide concrete guidance on how to achieve this required level of heterogeneity - an essential consideration in experimental settings where the researchers intervene in the covariates $X^{(e)}$ across different environments to uncover causal structures [He and Geng, 2008, Hauser and Bühlmann, 2015]. Moreover, invariance learning in structural equation models for inferring causality has been pioneered in Peters et al. [2016] and further developed in [Rothenhäusler et al., 2019, Shen et al., 2023], but the concrete causal identification conditions proposed along this line of works are often restrictive and challenging to implement in practice. Further discussions on these concrete conditions are provided in Section 1.3.

Beyond the gap in establishing causal identification conditions, the huge computation cost is another significant obstacle for existing causal invariance learning approaches, highlighting **(Q2)** as an open question. Existing methods, such as Peters et al. [2016], Ghassami et al. [2017], rely on exhaustive searches over all possible subsets of covariates to test the invariance of the outcome model, resulting in a computational complexity exponentially growing with the number of covariates. While Fan et al. [2023] solves invariant prediction models using a regularized least squares optimization, the inclusion of the indicator function in their objective function still necessitates an exhaustive enumeration of subsets. These approaches, whether explicitly or implicitly, frame causal invariance learning as *discrete integer programming*, leading to computational costs scaling exponentially with the dimension; see more discussions in Section 2.3. As a result, they become impractical for even moderately large p . For instance, as shown in our numerical experiments in Section 6, these methods [Peters et al., 2016, Fan et al., 2023] take over half an hour to complete when $p = 25$. See also Section 1.3 where we compare with other computationally feasible methods.

1.2 Our Results and Contributions

In this work, we focus on the additive intervention regime, a structured framework of generating heterogeneous multi-environment datasets [Rothenhäusler et al., 2019, 2021, Shen et al., 2023]. This regime characterizes the full data generation process for each environment via structural equation models (Definition 1), and attributes distributional heterogeneity by adding environment-specific perturbations to generate the covariate distributions; see the detailed introduction in Section 3.1.

The first main contribution of this work is addressing **(Q1)** by establishing concrete identification conditions for causal invariance learning. Specifically, we derive a nearly necessary and sufficient condition ensuring the uniqueness of the invariant prediction model. Such a condition enables causal discovery as the causal outcome model is guaranteed to be this unique invariant prediction model. Unlike the abstract heterogeneity conditions proposed in prior works [Fan et al., 2023, Yin et al., 2024], our identification condition directly leverages the covariate distributions across environments, and our assumptions are essentially necessary and hence weaker than in previous work [Rothenhäusler et al., 2019, Shen et al., 2023].

Building upon the identification conditions, we formulate causal invariance learning as a continuous nonconvex optimization problem, referred to as *Negative Weight Distributionally Robust Optimization* (NegDRO). NegDRO minimizes the worst-case combination of risks across multiple environments while allowing for negative weighted combinations. The inclusion of negative weights is critical in constructing invariant risk prediction across environments, which further leads to the causal discovery under our proposed identification conditions. A key contribution of this work is framing causal invariance learning as a contin-

uous nonconvex optimization problem, in contrast to the discrete integer programming approaches used in prior works [Peters et al., 2016, Ghassami et al., 2017, Fan et al., 2023]. Moreover, we demonstrate that the global optimizer of the nonconvex NegDRO recovers the true causal outcome model, providing a principled approach to causal discovery.

From an optimization perspective, the inclusion of negative weights breaks convexity, which distinguishes our work from classical group DRO [Sagawa et al., 2019], where the weights lie within a simplex. The nonconvex nature of NegDRO presents computational challenges in locating its global optimizer, which is about the fundamental limit of efficient computation highlighted in (Q2). We overcome this hurdle by demonstrating that any (generalized) stationary point of NegDRO, under causal identification conditions, is globally optimal, thereby recovering the causal outcome model. Leveraging this insight, we show that (sub)gradient descent algorithms, capable of computing stationary points of NegDRO, converge to the causal outcome model. Unlike exhaustive search approaches, our algorithm avoids the computational burdens of enumerating over all possible subsets of covariates and is scalable to scenarios involving a large number of variables, addressing (Q2). Furthermore, we establish the theoretical guarantees for the convergence of our algorithms to the causal outcome model with respect to both the sample size and iteration times.

Lastly, we validate our proposed algorithm through empirical studies, demonstrating its superior performance in terms of both estimation accuracy and computational efficiency within the additive intervention regime, compared to existing causal invariance learning methods.

To summarize, the main contributions of this paper are as follows:

1. We propose a general class of causal identification conditions in the additive intervention regime, and identify a nearly necessary and sufficient condition for ensuring the uniqueness of the invariant prediction model.
2. We formulate causal invariance learning as a continuous nonconvex optimization problem, whose global optimizer corresponds to the causal outcome model under the proposed identification condition.
3. We show that any (generalized) stationary point of NegDRO is globally optimal, under causal identification conditions, which leads to a computationally efficient algorithm for causal discovery.

1.3 Related Further Literature

Causal Invariance Learning. In addition to the above mentioned works, another line of research on causal discovery imposes concrete identification conditions that require a large number of heterogeneous environments. For example, Rojas-Carulla et al. [2018] demonstrates that causal discovery is achieved with an infinite number of environments covering all possible covariate interventions, while Arjovsky et al. [2019] requires at least $|\mathcal{E}| \geq p$ environments, where p is the number of covariates. However, generating numerous heterogeneous environments through interventions is often costly and impractical, limiting the applicability of these approaches. In contrast, our identification condition is much weaker and is nearly necessary and sufficient for ensuring the uniqueness of the invariant prediction model. Moreover, our identification condition demonstrates that causal discovery is achievable even with just two environments, regardless of the number of covariates p ; see Condition 2a for more details.

Causal Discovery for Additive Interventions. CausalDantzig [Rothenhäusler et al., 2019] and DRIG [Shen et al., 2023] identify the causal effect by matching the loss gradients across pairs of environments. In contrast, our approach essentially leverages the matching of risks across (all) different environments, which requires solving a nonconvex optimization problem. Their methodologies rely on assumptions, such as the non-singularity of Gram matrices or the availability of a reference environment. However, such assumptions are stronger and the settings more restrictive than ours. In contrast, our proposed NegDRO method remains

effective, achieving causal discovery in substantially greater generality. Further details and comparisons are provided in Section 5.2.

Group DRO and Maximin Effect. Group DRO [Sagawa et al., 2019, Wang et al., 2023] and Maximin Effects [Meinshausen and Bühlmann, 2015, Guo, 2024] minimize the worst-case combination of risks across environments, with the combination weights restricted to lie within a simplex. These methods are not intended to identify the causal outcome model, but construct prediction models that generalize well to unseen environments. NegDRO extends this framework by permitting *negative* combination weights, which enforce invariant risks across environments - a key property for identifying the causal outcome model. Meanwhile, the inclusion of negative weights results in a nonconvex optimization problem, a complexity which is not encountered in these earlier methods. As one of our key contributions, we develop a computationally efficient algorithm to solve this nonconvex optimization problem and thus achieve causal discovery.

Global Optimality of Nonconvex Optimization. Achieving global optimality in nonconvex optimization is notoriously challenging, as exhaustive search methods often exhibit exponential dependence on the problem dimension. Recent advancements in nonconvex optimization have leveraged structured landscape properties to establish global convergence for gradient-based methods. Key conditions facilitating such results include hidden convexity [Ben-Tal and Teboulle, 1996], the Polyak-Lojasiewicz (PL) condition [Polyak et al., 1963, Lojasiewicz, 1963], the Kurdyka-Lojasiewicz (KL) condition [Kurdyka, 1998], and other gradient dominance properties [Karimi et al., 2016]. Hidden convexity suggests the existence of a convex reformulation via a variable change, enabling efficient algorithmic solutions [Fatkhullin et al., 2023, Chen et al., 2024a]. The PL, KL, and other gradient dominance conditions ensure that any stationary point is globally optimal, which allows gradient-based methods to converge globally [Fatkhullin et al., 2022]. However, verifying these properties is often highly non-trivial and typically requires a case-by-case investigation. Examples of such investigations can be found in Markov decision processes and operations problems [Feng and Shanthikumar, 2018, Lan, 2023, Klein et al., 2023, Chen et al., 2024b]. For a more comprehensive list of efficiently solvable nonconvex problems, we refer interested readers to Sun [2021]. To the best of our knowledge, the causal invariance learning problem considered in this work does not admit any of these established properties. We frame causal invariance learning as a continuous nonconvex optimization problem, termed NegDRO. By exploiting the unique structure of the causal outcome model and the associated identification conditions, we develop a novel analysis demonstrating that any (generalized) stationary point of the NegDRO problem is globally optimal. As a result, standard gradient-based algorithms designed to find stationary points can achieve efficient convergence to global optimality in this setting.

Out-of-distribution Generalization. Inspired by causal invariance learning, approaches such as “Invariant Risk Minimization” (IRM) [Arjovsky et al., 2019] and its variants [Chuang et al., 2020, Lu et al., 2021, Liu et al., 2021] focus on finding data representations where optimal predictors remain invariant across all environments, and such techniques have been applied extensively in machine learning. “Minimax Risk Extrapolation” (MM-REx) [Krueger et al., 2021] leverages the risk invariance principle, aligning conceptually with our NegDRO, but emphasizes minimizing the variance of environments’ risks. Despite some reported and partially debated empirical success, the methods’ theoretical understanding remains limited [Rosenfeld et al., 2020, Kamath et al., 2021]. In contrast, our work focuses on linear models, providing theoretical analysis including identification conditions, as well as computationally efficient algorithms with rigorous convergence guarantees. Our results serve as a stepping stone for advancing causal invariance learning in more complex, nonlinear scenarios.

Directed Acyclic Graphs (DAGs). When the causal structure is unknown, DAG-based methods provide another framework to infer causal relationships among variables [Verma and Pearl, 1990, Andersson et al., 1997, Chickering, 2002, Kalisch and Bühlman, 2007, Hauser and Bühlmann, 2012, 2015, Eberhardt et al., 2024, Taeb et al., 2024]. These approaches aim to construct the entire causal structure of all observed

variables (or its Markov equivalence class) by leveraging the conditional independence relationships to distinguish between equivalent structures. In contrast, our work focuses on identifying the causal outcome model, specifically targeting the direct causal effect from covariates to the outcome, rather than constructing the entire causal graph. The causal invariance learning can be viewed as an alternative pathway of identifying the causal outcome, requiring different identification conditions and computational algorithms than the ones from the DAG literature.

1.4 Preliminaries, Notations and Outline

In the following, we provide a brief review of several important concepts in causal inference that facilitate the discussion of the current paper, and introduce the notations that will be used throughout this paper.

We start with the structural equation model (SEM) [Pearl, 2009, Bollen, 2014], also known as the structural causal model (SCM) [Pearl et al., 2016], that is commonly used to characterize the causal relationship.

Definition 1 (Structural Equation Models). We consider the SEM on variables $Z = (Z_1, Z_2, \dots, Z_{p+1})$ with

$$Z_j = f_j(\text{Pa}(Z_j), \varepsilon_j) \quad \text{for } 1 \leq j \leq p + 1,$$

where the set $\text{Pa}(Z_j) \subseteq \{Z_1, \dots, Z_{p+1}\}$ denotes the set of direct causes of Z_j , or *parents*, of the variables, and ε_j represents the random error or disturbance due to omitted factors.

When all functions f_j 's are linear, these SEMs are referred to as linear SEMs. The SEMs in Definition 1 naturally induce a directed causal graph $G = (V, E)$, within the framework of causal graphical models [Pearl, 2009, Spirtes et al., 2001]. Here $V = \{1, \dots, p + 1\}$ represents the set of nodes (vertices), and E represents the set of directed edges, where $(i, j) \in E$ if and only if node i is the parent of j . A node j is said to be a (direct) *child* of node i if and only if i is a parent of j .

Definition 2 (Causal Graph). We say there is a *directed path* from node i to j if there exists a sequence of nodes (v_1, \dots, v_k) with $k \geq 2$ such that $v_1 = i$, $v_k = j$, and $(v_l, v_{l+1}) \in E$ for any $1 \leq l \leq k - 1$. We call a directed graph G is a *directed acyclic graph* (DAG) if there does not exist a directed path from node j to itself for any node $j \in V$. Any node connected by a directed path to i is an *ancestor* of i , and any node connected by a directed path from i is a *descendant* of i .

We now introduce the notations used in this paper. For a set S , we use $|S|$ to denote its cardinality, and $\text{Pow}(S) = \{A : A \subseteq S\}$ to denote its power set. Define $[m] = \{1, 2, \dots, m\}$ for the positive integer m . For real numbers a and b , define $a \wedge b = \min\{a, b\}$ and $a \vee b = \max\{a, b\}$. We use c and C to denote generic positive constants that may vary from place to place. For positive sequences $a(n)$ and $b(n)$, we use $a(n) \lesssim b(n)$, $a(n) = \mathcal{O}(b(n))$ or $b(n) = \Omega(a(n))$ to represent that there exists some universal constant $C > 0$ such that $a(n) \leq C \cdot b(n)$ for all $n \geq 1$, and denote $a(n) \asymp b(n)$ if $a(n) \lesssim b(n)$ and $b(n) \lesssim a(n)$. We use notations $a(n) \ll b(n)$ or $a(n) = o(b(n))$ if $\limsup_{n \rightarrow \infty} (a(n)/b(n)) = 0$. For a vector $x \in \mathbb{R}^p$ and a set $S \subseteq [p]$, x_S represents the $|S|$ -dimensional sub-vector of x consisting of x_j 's for all $j \in S$. We use $\text{supp}(x) = \{j \in [p] \mid x_j \neq 0\}$ to denote the support set of the vector x . For $q \geq 0$, let $\|x\|_q = (\sum_{i=1}^p |x_i|^q)^{1/q}$ be its ℓ_q norm. When there is no ambiguity, we use $\|x\|$ to represent the ℓ_2 norm of the vector x by default. For a matrix $A = [A_{i,j}]_{i \in [n], j \in [m]}$, we denote $A_{S_1, S_2} = [A_{i,j}]_{i \in S_1, j \in S_2}$ as the sub-matrix of A . We let $\|A\|_2$ be the spectral norm of matrix A , and may abbreviate it as $\|A\|$ when there is no ambiguity. We define $\text{Dist}(x, A) := \min_{x' \in A} \|x' - x\|_2$ for any set A . We use \mathbf{I}_p to denote the p -dimensional identity matrix. For two random variables X, Y , we use $X \stackrel{d}{=} Y$ to indicate they share the same distribution.

The structure of the paper is outlined as follows. In Section 2, we provide a detailed introduction to the causal invariance learning problem and present the formulation of NegDRO. Building on this, Section

3 introduces the additive intervention regime, specifies the identification condition for causal discovery, and shows that the global optimizer of NegDRO recovers the causal outcome model. In Section 4, we propose a computationally efficient algorithm to achieve causal discovery and establish the convergence rate of our algorithm output. Following this, Section 5 explores a scenario with limited interventions, and compares NegDRO with existing approaches specifically designed for the additive intervention regime. Finally, Section 6 presents numerical results validating our arguments.

2 Causal Invariance Learning and Negative Weight DRO

Throughout the paper, we focus on the regime that we have access to data collected from multiple environments $\mathcal{E} = \{1, \dots, |\mathcal{E}|\}$, with $|\mathcal{E}|$ denoting the total number of environments. For each environment $e \in \mathcal{E}$, we observe the data $\{x_i^{(e)}, y_i^{(e)}\}_{i=1}^{n_e}$, which are identically and independently distributed (i.i.d) drawn from the distribution of $(X^{(e)}, Y^{(e)})$, where $X^{(e)} \in \mathbb{R}^p$ and $Y^{(e)} \in \mathbb{R}$ respectively denote the covariates and the outcome in the e -th environment.

2.1 Invariant Causal Outcome Model

We assume that for all $e \in \mathcal{E}$, there exists a subset $S^* \subseteq [p]$, such that $X_{S^*}^{(e)}$ are direct causes of $Y^{(e)}$, that is, a structural equation

$$Y^{(e)} = (\beta_{S^*}^*)^\top X_{S^*}^{(e)} + \varepsilon_Y^{(e)}, \quad (1)$$

where $\beta^* \in \mathbb{R}^p$ represents the causal effect with $\beta_{(S^*)^c}^* = 0$ and $\varepsilon_Y^{(e)}$ encodes other (unobserved) factors that affect the outcome variable. Notably, the remaining covariates $X_{(S^*)^c}^{(e)}$ are not direct causes or may even be caused by $Y^{(e)}$, and we allow the existence of unmeasured confounders $\mathbb{E}[\varepsilon_Y^{(e)} | X_{S^*}^{(e)}] \neq 0$. We consider the following example to illustrate the model (1) and further demonstrate it in Figure 1.

Example 1. For each environment $e \in \mathcal{E}$, the variables $(X^{(e)}, Y^{(e)})$ are generated as follows:

$$X_1^{(e)} = \varepsilon_1^{(e)}, \quad Y^{(e)} = X_1^{(e)} + \varepsilon_Y^{(e)}, \quad X_2^{(e)} = Y^{(e)} + \varepsilon_2^{(e)}, \quad (2)$$

$$\text{where } (\varepsilon_1^{(e)}, \varepsilon_2^{(e)})^\top \sim \mathcal{N}(0, \sigma^{(e)} \mathbf{I}_2), \quad \text{and } \varepsilon_Y^{(e)} \sim \mathcal{N}(0, 1) \text{ are jointly independent.} \quad (3)$$

As demonstrated in Figure 1, only $X_1^{(e)}$ is the direct cause of $Y^{(e)}$ with $S^* = \{1\}$ and $\beta^* = (1, 0)$, even though $X_2^{(e)}$ is also associated with the outcome.



Figure 1: Illustration of (1) in Example 1 with $S^* = \{1\}$.

In this paper, we aim at identifying the causal effect β^* using the data from multiple environments. However, the identification of β^* is a challenging task, due to the absence of prior knowledge about the causal ordering between the outcome of interest and the observed covariates. Some of the observed covariates might cause the outcome while others might be further affected by the outcome. For instance, in Example 1, $X_1^{(e)}$ causes $Y^{(e)}$ but $Y^{(e)}$ causes $X_2^{(e)}$. In practice, we only have access to the observations of $Y^{(e)}, X_1^{(e)}, X_2^{(e)}$ without knowing their causal ordering. A majority of causal inference literature assumes a known causal ordering between Y and X and mainly focuses on estimating the magnitude of β^* [Wooldridge, 2009, Imbens and Rubin, 2015, Morgan, 2015]. For example, in the randomized experiment, the treatment precedes

the outcome, establishing a natural causal ordering before learning the treatment effect. In contrast, the current paper does not assume prior knowledge of the causal ordering but aims to devise a data-dependent way of learning the set S^* of covariates that cause Y , from the observed data only. An additional challenge in recovering β^* is the existence of unmeasured confounding with $\mathbb{E}[\varepsilon_Y^{(e)} | X_{S^*}^{(e)}] \neq 0$. In such cases, even if we know S^* , β^* differs from the best linear projection $\arg \min_{\text{supp}(b)=S^*} \mathbb{E}[Y^{(e)} - b^\top X^{(e)}]^2$, which requires additional identification conditions for recovering β^* in the presence of unmeasured confounding.

The identification of β^* becomes challenging when the causal ordering is unknown or unmeasured confounders are present. To enable causal identification in such regimes, we leverage the invariance principle: the causal relationship in (1) is assumed to remain invariant, while the distributions of the covariates change across different environments. By distinguishing between the invariant outcome model and the heterogeneous covariate distributions, we identify the causal model β^* in (1); see Section 2.2 for an illustrative example. This general invariance principle has proven effective in learning S^* and $\beta_{S^*}^*$ by leveraging the data from multiple environments [Peters et al., 2016, Ghassami et al., 2017, Rothenhäusler et al., 2019, Fan et al., 2023]. We now introduce a specific version of the invariance principle and comment on its connections to existing work.

The model (1) holds for all $e \in \mathcal{E}$ with $\mathbb{E}[(\varepsilon_Y^{(e)})^2] = \sigma_Y^2$ for some constant $\sigma_Y^2 > 0$. (Invariance Principle)

The above [Invariance Principle](#) requires that the residual errors share the same second-order moment across different environments, that is,

$$\forall e, f \in \mathcal{E}, \quad \mathbb{E} \left[Y^{(e)} - (\beta_{S^*}^*)^\top X_{S^*}^{(e)} \right]^2 = \mathbb{E} \left[Y^{(f)} - (\beta_{S^*}^*)^\top X_{S^*}^{(f)} \right]^2.$$

Other versions of the invariance principle have been proposed in the literature. Peters et al. [2016], Rojas-Carulla et al. [2018] considered an invariance condition where the conditional distribution $Y^{(e)} | X_{S^*}^{(e)}$ remains the same across environments. This condition is also termed as ‘‘autonomy’’, ‘‘modularity’’ [Haavelmo, 1944, Aldrich, 1989] and ‘‘stability’’ [Dawid and Didelez, 2010]. Such an invariance condition implies our [Invariance Principle](#) that mainly requires the identical noise level instead of the whole conditional distribution. Moreover, other multi-environment studies [Pfister et al., 2021, Fan et al., 2023, Yin et al., 2024] impose another invariance principle assuming the conditional mean $\mathbb{E}[Y^{(e)} | X_{S^*}^{(e)}]$ to stay identical across environments. These approaches are built under the no unmeasured confounder assumption $\mathbb{E}[\varepsilon_Y^{(e)} | X_{S^*}^{(e)}] = 0$, for all $e \in \mathcal{E}$. However, our model ([Invariance Principle](#)) allows $\mathbb{E}[\varepsilon_Y^{(e)} | X_{S^*}^{(e)}] \neq 0$, accommodating the existence of unmeasured confounding between the outcome $Y^{(e)}$ and its parents $X_{S^*}^{(e)}$.

Finally, we define a prediction model b to be an invariant prediction model across environments $e \in \mathcal{E}$ if $\mathbb{E}[(Y^{(e)} - b^\top X^{(e)})^2] = \mathbb{E}[(Y^{(f)} - b^\top X^{(f)})^2]$ for $e, f \in \mathcal{E}$. We further define the set of invariant prediction models across environments in \mathcal{E} as

$$\mathcal{B}_{\text{inv}}(\mathcal{E}) := \left\{ b \in \mathbb{R}^p : \mathbb{E}(Y^{(e)} - b^\top X^{(e)})^2 = \mathbb{E}(Y^{(f)} - b^\top X^{(f)})^2, \forall e, f \in \mathcal{E} \right\}. \quad (4)$$

Note that, when the [Invariance Principle](#) holds, the causal model β^* belongs to $\mathcal{B}_{\text{inv}}(\mathcal{E})$.

2.2 An Illustrative Example for Causal Invariance Learning

We now use Example 1 to demonstrate how to identify β^* via contrasting the invariant causal outcome model against heterogeneous environments. For illustration purposes, we consider two environments $\mathcal{E} = \{1, 2\}$ with distinct noise levels $\sigma^{(1)} \neq \sigma^{(2)}$ as specified in (3). Inspired by the ICP framework [Peters et al., 2016], we test compliance with the risk invariance principle in all possible subsets of covariates.

To illustrate the main idea, we perform the computation at the population level. For each subset $S \in \{\emptyset, \{1\}, \{2\}, \{1, 2\}\}$, we run a regression $Y^{(e)}$ on $X_S^{(e)}$ to obtain the best linear prediction model \bar{b}_S and input all other entries of \bar{b} with zeros. For $S \in \{\emptyset, \{1\}, \{2\}, \{1, 2\}\}$, we then compute the corresponding risk $\mathbb{E}[\ell(X^{(e)}, Y^{(e)}; \bar{b})]$ for the e -th environment. The results are summarized in Table 1. The subset $S = \{1\}$

S	\emptyset	$\{1\}$	$\{2\}$	$\{1, 2\}$
\bar{b}	$(0, 0)^\top$	$(1, 0)^\top$	$\left(0, \frac{(\sigma^{(e)})^2 + 1}{2(\sigma^{(e)})^2 + 1}\right)^\top$	$\left(\frac{(\sigma^{(e)})^2}{(\sigma^{(e)})^2 + 1}, \frac{1}{(\sigma^{(e)})^2 + 1}\right)^\top$
$\mathbb{E}[\ell(X^{(e)}, Y^{(e)}; \bar{b})]$	$(\sigma^{(e)})^2 + 1$	1	$\frac{(\sigma^{(e)})^4 + (\sigma^{(e)})^2}{2(\sigma^{(e)})^2 + 1}$	$\frac{(\sigma^{(e)})^2}{(\sigma^{(e)})^2 + 1}$

Table 1: We consider Example 1 and report the best population prediction model \bar{b} using the covariates belonging to S , together with the environment specific risk $\mathbb{E}[\ell(X^{(e)}, Y^{(e)}; \bar{b})]$.

produces a prediction model $\bar{b} = (1, 0)^\top$, with an invariant risk $\mathbb{E}[\ell(X^{(e)}, Y^{(e)}; \bar{b})] = 1$ across environments. In contrast, all other subsets lead to a violation of the invariance principle, as their risks vary across different environments. Consequently, we identify the causal set $S^* = \{1\}$ and the causal effect $\beta^* = (1, 0)^\top$. We shall comment that the idea presented above is essential to implement an exhaustive searching algorithm, which is inherently difficult to scale up with a large number of covariates. We mainly use such an exhaustive searching algorithm to demonstrate how to learn the causal outcome model conceptually. We introduce a continuous (nonconvex) optimization problem for learning the true causal model β^* and further devise a computationally efficient algorithm for causal discovery in the following Section 4.

2.3 Optimization Formulation

As demonstrated in Section 2.2, most existing causal invariance learning methods rely on exhaustive searches over all possible subsets of covariates, checking each of the 2^p subsets for compliance with the invariance principle. For example, “Invariant Causal Prediction” (ICP) [Peters et al., 2016] involves enumerating and running regressions on every subset $S \subseteq [p]$, and incorporates multiple hypothesis testing throughout the process. Subsequent works, such as Ghassami et al. [2017], Heinze-Deml et al. [2018], Rojas-Carulla et al. [2018], Pfister et al. [2019] follow the similar hypothesis-testing approach for causal discovery. Fan et al. [2023] introduced the “Environment Invariant Linear Least Squares”(EILLS) method to estimate β^* through regularized least squares optimization, given by:

$$\arg \min_{b \in \mathbb{R}^p} \sum_{e \in \mathcal{E}} \mathbb{E}[(Y^{(e)} - b^\top X^{(e)})^2] + \gamma \sum_{j=1}^p \mathbf{1}\{b_j \neq 0\} \times \sum_{e \in \mathcal{E}} \left| \mathbb{E}[(Y^{(e)} - b^\top X^{(e)})X_j^{(e)}] \right|^2.$$

The use of the indicator function $\mathbf{1}\{b_j \neq 0\}$ in their objective function still requires enumerating every subset $S \subseteq [p]$. These approaches, whether explicitly or implicitly, frame causal invariance learning as an integer programming problem by enumerating all subsets $S \subseteq [p]$, resulting in a computational complexity that scales exponentially with the dimension p . Consequently, implementing such exhaustive search algorithms becomes impractical for even moderately large p ; see the numerical results in Section 6 for instance.

To address the computational challenge, we propose a novel continuous optimization formulation for causal discovery, designed to sidestep the need for exhaustive search. Specifically, we formulate the problem as a minimax optimization model, inspired by the idea of distributionally robust optimization (DRO) [Ben-Tal et al., 2013, Namkoong and Duchi, 2016]. For a given $\gamma \geq 0$, we define the following set $\mathcal{U}(\gamma)$:

$$\mathcal{U}(\gamma) = \left\{ w \in \mathbb{R}^{|\mathcal{E}|} : \sum_{e \in \mathcal{E}} w_e = 1, \min_{e \in \mathcal{E}} w_e \geq -\gamma \right\}. \quad (5)$$

With the above set, we consider the following minimax optimization problem,

$$b_{\text{Neg}}^\gamma = \arg \min_{b \in \mathbb{R}^p} \max_{w \in \mathcal{U}(\gamma)} \sum_{e \in \mathcal{E}} w_e \mathbb{E}[\ell(X^{(e)}, Y^{(e)}; b)], \quad (6)$$

where $\ell(x, y; b) = (y - b^\top x)^2$ stands for the squared-loss function, and we refer to $\mathbb{E}[\ell(X^{(e)}, Y^{(e)}; b)]$ as the risk in e -th environment. We refer to the minimax optimization in (6) as *Negative weight DRO* (NegDRO), since some environments may be assigned negative weights. When $\gamma = 0$, the optimization problem in (6) is reduced to the group DRO [Sagawa et al., 2019, Hashimoto et al., 2018]. However, when $\gamma > 0$, the NegDRO problem in (6) is fundamentally different from the group DRO [Sagawa et al., 2019, Hashimoto et al., 2018] as the optimization problem in (6) becomes nonconvex. Similarly to the generalization property of DRO, the NegDRO algorithm tends to produce more generalizable prediction models for unseen future environments, compared to the empirical risk minimization (ERM) method, which optimizes the weighted average of the risk function with the weight being proportional to the sample sizes.

We shall emphasize that, for a positive $\gamma > 0$, the objective $\sum_e w_e \mathbb{E}[\ell(X^{(e)}, Y^{(e)}; b)]$ in (6) becomes a nonconvex function with respect to b , since its Hessian matrix $\sum_e w_e \mathbb{E}[X^{(e)}(X^{(e)})^\top]$ is not necessarily positive semi-definite in the presence of some negative weights w_e . In general, the NegDRO problem in (6) is a minimax optimization problem with a nonconvex concave objective, and it is challenging to obtain the global optimizer of such nonconvex optimization problems [Boyd and Vandenberghe, 2004, Bonnans et al., 2006]. More discussions about nonconvex concave minimax optimization will be provided in the following Remark 1. As our main contribution, we devise a computationally efficient algorithm to obtain the global optimizer of NegDRO in the following Section 4.2.

Next, we provide the intuition for why the NegDRO in (6) encourages an invariant prediction model for a large regularization parameter $\gamma > 0$. After solving the inner optimization problem of (6), we admit the following equivalent form of the NegDRO problem in (6):

$$b_{\text{Neg}}^\gamma = \arg \min_{b \in \mathbb{R}^p} \left\{ \max_{e \in \mathcal{E}} \mathbb{E}[\ell(X^{(e)}, Y^{(e)}; b)] + \gamma |\mathcal{E}| \cdot \left(\max_{e \in \mathcal{E}} \mathbb{E}[\ell(X^{(e)}, Y^{(e)}; b)] - \frac{1}{|\mathcal{E}|} \sum_{f \in \mathcal{E}} \mathbb{E}[\ell(X^{(f)}, Y^{(f)}; b)] \right) \right\}. \quad (7)$$

The equivalence between (6) and (7) holds due to the fact that the maximization over the linear weight w in (6) is attained if we assign the weight $1 + \gamma(|\mathcal{E}| - 1)$ to the environment with the largest risk, and assign the weights $-\gamma$ to all other environments. Given a predictor $b \in \mathbb{R}^p$, the objective in (7) balances the largest risk among environments and the discrepancy between the largest and average environments' risks, mediated by the regularization parameter γ . When $\gamma = 0$, it aims to minimize the largest risk among all observed environments. As γ increases, the model strives for risk parity across environments, encouraging the discrepancy of environments' risks to be smaller, and minimizes the largest environment's risk meanwhile. When $\gamma = \infty$, b_{Neg}^γ is forced to have the invariant risks across all observed environments: $\mathbb{E}[\ell(X^{(e)}, Y^{(e)}; b_{\text{Neg}}^\gamma)] = \mathbb{E}[\ell(X^{(f)}, Y^{(f)}; b_{\text{Neg}}^\gamma)]$, for any pairs of $e, f \in \mathcal{E}$. Hence, for $\gamma = \infty$, the global optimizer of (7), denoted as b_{Neg}^∞ , admits the following form:

$$b_{\text{Neg}}^\infty = \arg \min_{b \in \mathbb{R}^p} \mathbb{E}[\ell(X^{(e)}, Y^{(e)}; b)] \quad \text{s.t.} \quad \mathbb{E}[\ell(X^{(e)}, Y^{(e)}; b)] = \mathbb{E}[\ell(X^{(f)}, Y^{(f)}; b)] \quad \forall e, f \in \mathcal{E}. \quad (8)$$

Recall that the causal parameter β^* admits the invariant risk across environments as well, as shown in the [Invariance Principle](#). Therefore, both b_{Neg}^∞ and β^* belong to the set of risk-invariant prediction models \mathcal{B}_{inv} as defined in (4). In the following Section 3.2, we shall introduce the nearly necessary and sufficient condition ensuring that β^* is the unique invariant risk prediction model such that $\mathcal{B}_{\text{inv}} = \{\beta^*\}$. This further implies that our proposed b_{Neg}^∞ matches the causal parameter β^* . Additionally, for general finite $\gamma \geq 0$, we establish in Section 3.3 that b_{Neg}^γ converges to β^* with an increasing value of γ .

We now conclude this section with an additional remark discussing minimax optimization.

Remark 1 (Minimax Optimization). In the case of standard convex-concave minimax optimization, a vast amount of literature has already shown the convergence to the global optimum via classical gradient-based methods [Korpelevich, 1976, Chen and Rockafellar, 1997, Nemirovski, 2004, Auslender and Teboulle, 2009, Nedić and Ozdaglar, 2009, Lin et al., 2020, Rahimian and Mehrotra, 2022]. Recently, there is a growing interest in solving nonconvex concave minimax optimization [Heusel et al., 2017, Rafique et al., 2022, Lin et al., 2024], where most existing algorithms, such as two-timescale gradient descent-ascent [Lin et al., 2024], are guaranteed to converge to a local minimum, while the global optimizer remains mysterious. We shall emphasize that the nonconvexity in the proposed NegDRO problem (6) arises from the possibly negative weights instead of the generic nonconvex function as studied in the works Heusel et al. [2017], Lin et al. [2024]. By leveraging the causal identification condition introduced in Conditions 1 and 2a, we successfully characterize the global optimizer of the nonconvex concave NegDRO problem. This fundamental distinction sets our work apart from prior studies, where global optimality remains an open challenge.

3 Additive Intervention and Identification Conditions

We introduce in Section 3.1 the additive intervention regime, which is commonly used to generate multi-environment data used for causal invariance learning. In Section 3.2, we introduce an identification condition for causal discovery. Lastly, in Section 3.3, we establish the convergence of the global optimal solution b_{Neg}^γ in (6) to the causal effect β^* .

3.1 Additive Intervention

In the following, we introduce the additive intervention regime as a concrete way of generating heterogeneous multi-source data sets, as adopted in prior works [Hoyer et al., 2008, Janzing and Schölkopf, 2010, Daniusis et al., 2012, Janzing et al., 2012, Peters et al., 2014, Ghassami et al., 2017, Rothenhäusler et al., 2019, 2021, Shen et al., 2023, Polinelli et al., 2024]. For each environment $e \in \mathcal{E}$, the data-generating process of $(X^{(e)}, Y^{(e)})$ follows the structural equation model (SEM) given by:

$$\begin{pmatrix} Y^{(e)} \\ X^{(e)} \end{pmatrix} = \mathbf{B} \begin{pmatrix} Y^{(e)} \\ X^{(e)} \end{pmatrix} + \begin{pmatrix} \varepsilon_Y^{(e)} \\ \varepsilon_X^{(e)} \end{pmatrix}, \quad \text{with } \mathbf{B} = \begin{pmatrix} 0 & (\beta^*)^\top \\ \mathbf{B}_{YX} & \mathbf{B}_{XX} \end{pmatrix}, \quad (9)$$

where \mathbf{B} characterizes the relationships among X and Y and $(\varepsilon_Y^{(e)}, \varepsilon_X^{(e)})$ are the environment-specific errors. The above SEMs incorporate the causal outcome model (1) as a component and further provide the generating distribution of the covariates $X^{(e)}$. In (9), β^* is the causal effect of interest, $\mathbf{B}_{YX} \in \mathbb{R}^p$ describes the effect of the outcome $Y^{(e)}$ on the covariates $X^{(e)}$, and $\mathbf{B}_{XX} \in \mathbb{R}^{p \times p}$ captures interrelationships among covariates themselves. We illustrate the SEM in (9) with concrete examples. In Example 1, $X_1^{(e)}$ is the sole cause of $Y^{(e)}$, resulting in $\beta^* = (1, 0)^\top$; $Y^{(e)}$ directly causes $X_2^{(e)}$, leading to $\mathbf{B}_{YX} = (0, 1)^\top$. There are no direct causal relationships among covariates, making $\mathbf{B}_{XX} = 0_{2 \times 2}$. To further elucidate each component of the matrix \mathbf{B} , we consider the following Example 2, whose causal diagram is depicted in Figure 2.

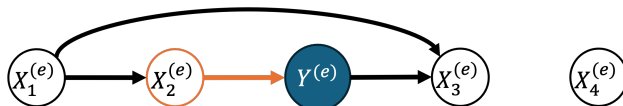


Figure 2: Illustration of the SEM (9) for Example 2, where the highlighted orange covariate $X_2^{(e)}$ is the sole direct cause of the outcome $Y^{(e)}$.

Example 2. For each environment $e \in \mathcal{E}$, the variables $(X^{(e)}, Y^{(e)})$ are generated as follows:

$$X_1^{(e)} = \varepsilon_1^{(e)}, \quad X_2^{(e)} = X_1^{(e)} + \varepsilon_2^{(e)}, \quad Y^{(e)} = 2X_2^{(e)} + \varepsilon_Y^{(e)}, \quad X_3^{(e)} = 0.5X_1^{(e)} - Y^{(e)} + \varepsilon_3^{(e)}, \quad X_4^{(e)} = \varepsilon_4^{(e)},$$

where $\varepsilon_1^{(e)}, \varepsilon_2^{(e)}, \varepsilon_3^{(e)}, \varepsilon_4^{(e)}, \varepsilon_Y^{(e)}$ represent random noises.

Among the four covariates, $X_2^{(e)}$ is the *only* direct cause of $Y^{(e)}$, establishing the causal set $S^* = \{2\}$ and defining the causal effect vector as $\beta^* = (0, 2, 0, 0)$. The outcome $Y^{(e)}$ directly causes $X_3^{(e)}$ but no other covariates, yielding $\mathbf{B}_{YX} = (0, 0, -1, 0)^\top$. Furthermore, there exist causal interactions among covariates themselves, with $[\mathbf{B}_{XX}]_{2,1} = 1, [\mathbf{B}_{XX}]_{3,1} = 0.5$, while all other entries in \mathbf{B}_{XX} are equal to zero. Notably, $[\mathbf{B}_{XX}]_{i,j} \neq 0$ if and only if $X_j^{(e)}$ is a direct cause of $X_i^{(e)}$. Here, $X_4^{(e)}$ is an isolated covariate, which has no directed causal path with both $Y^{(e)}$ and the remaining covariates.

In the additive intervention regime, the covariate distribution heterogeneity arises from the distributional shift of the noise $\varepsilon_X^{(e)}$. Following previous works [Rothenhäusler et al., 2019, 2021, Shen et al., 2023], we consider the following noise decomposition of $(\varepsilon_Y^{(e)}, \varepsilon_X^{(e)}) \in \mathbb{R}^{p+1}$,

$$\begin{pmatrix} \varepsilon_Y^{(e)} \\ \varepsilon_X^{(e)} \end{pmatrix} \stackrel{d}{=} \begin{pmatrix} \eta_Y \\ \eta_X \end{pmatrix} + \begin{pmatrix} 0 \\ \delta^{(e)} \end{pmatrix} \quad \text{with} \quad \mathbb{E}[\eta(\delta^{(e)})^\top] = 0, \quad (10)$$

where $\eta = (\eta_Y, \eta_X)^\top \in \mathbb{R}^{p+1}$, with $\eta_Y \in \mathbb{R}$ and $\eta_X \in \mathbb{R}^p$, denotes the systematic random error shared across environments and $\delta^{(e)} \in \mathbb{R}^p$ stands for the environment-specific perturbations added to the environment e . Here, the notation $\stackrel{d}{=}$ indicates two random variables share the same distribution.

In the error decomposition model (10), the outcome is not directly intervened, ensuring the **Invariance Principle** holds with $\mathbb{E}[(\varepsilon_Y^{(e)})^2] = \mathbb{E}[\eta_Y^2]$. Moreover, the systematic random error η shared across environments and the environment-specific noise $\delta^{(e)}$ are assumed to be uncorrelated with each other. The additive intervention defined in (10) indicates that the distributional heterogeneity across environments stems from the additive noise $\delta^{(e)}$, which justifies the name for the additive intervention as the whole distributional shift is driven by the additive component $\delta^{(e)}$. We summarize the data-generating process in the additive intervention regime in the following condition:

Condition 1 (Additive intervention). For each environment $e \in \mathcal{E}$, the random variables $(X^{(e)}, Y^{(e)})$ are generated following (9) and (10).

In this setup, the SEMs in (9) not only encompass the causal outcome model, as specified in **Invariance Principle**, but also characterize the full data generation process for each observed environment. We now provide more discussions on the error decomposition model in (10), which is broadly applicable to diverse scenarios. As a thought experiment, researchers might begin with a reference environment, where the random noises $(\varepsilon_Y, \varepsilon_X)^\top$ follow the distribution of η without intervention. For the e -th environment, researchers introduce the intervention $\delta^{(e)}$ to the covariates. Once the system stabilizes, they collect data from the e -th intervened environment. Here, the added intervention $\delta^{(e)}$ encodes various forms of distributional shifts in the covariates. For instance, consider the case where $\delta^{(e)} \sim \mathcal{N}(\mu^{(e)}, \Sigma^{(e)})$, then $\mu^{(e)} \neq 0$ represents a mean shift, while $\Sigma^{(e)} \neq 0$ represents a variance shift on the covariates distribution of $X^{(e)}$.

Moreover, the error decomposition model (10) incorporates scenarios involving hidden confounding among the noise terms $(\varepsilon_Y^{(e)}, \varepsilon_X^{(e)})$. Specifically, when unobserved variables simultaneously affect both η_Y and η_X , we have $\mathbb{E}[\varepsilon_Y^{(e)} \varepsilon_X^{(e)}] = \mathbb{E}[\eta_Y \eta_X] \neq 0$. This relaxes the no unmeasured confounding assumptions in prior works [Peters et al., 2014, Ghassami et al., 2017], assuming independent $\varepsilon_Y^{(e)}$ and $\varepsilon_X^{(e)}$.

As a final remark, we focus on the acyclic graph structure in the sense that there is no direct path from one variable to itself in the directed graph model induced by (9). Throughout the paper, we consider that the

SEM (9) generates an acyclic causal graph, ensuring that the matrix $\mathbf{I} - \mathbf{B}$ is invertible [Spirites et al., 2001, Pearl, 2009, Rothenhäusler et al., 2019]. Then, the SEM in (9) is expressed as follows:

$$\begin{pmatrix} Y^{(e)} \\ X^{(e)} \end{pmatrix} = (\mathbf{I} - \mathbf{B})^{-1} \begin{pmatrix} \varepsilon_Y^{(e)} \\ \varepsilon_X^{(e)} \end{pmatrix}. \quad (11)$$

The acyclic graph assumption also implies that the reverse causal effect \mathbf{B}_{YX} must have a disjoint support with S^* . In fact, the support of \mathbf{B}_{YX} is disjoint with all ancestors of the outcome variable; otherwise, the induced causal graph becomes acyclic.

3.2 Causal Identification Condition

In this subsection, we propose the nearly necessary and sufficient condition for when the set of risk-invariant prediction models, \mathcal{B}_{inv} , defined in (4), uniquely identifies the causal effect β^* under additive interventions. The causal identification condition is as follows.

Condition 2a. There exist two nonempty and disjoint collections of environments $\mathcal{E}_1, \mathcal{E}_2 \subseteq \mathcal{E}$, and some weights $w \in \Delta^{|\mathcal{E}_1|}$ and $w' \in \Delta^{|\mathcal{E}_2|}$ such that

$$\sum_{e \in \mathcal{E}_1} w_e \mathbb{E}[\delta^{(e)} \delta^{(e)\top}] \succ \sum_{f \in \mathcal{E}_2} w'_f \mathbb{E}[\delta^{(f)} \delta^{(f)\top}]. \quad (12)$$

The inequality (12) indicates that a weighted average intervention strength in one collection of environments \mathcal{E}_1 is strictly larger than that in another collection \mathcal{E}_2 . Importantly, the specific weights $w \in \Delta^{|\mathcal{E}_1|}$ and $w' \in \Delta^{|\mathcal{E}_2|}$ in (12) do not need to be known a priori, only their existence is required. This condition ensures that sufficient heterogeneity exists among environments, which is crucial for identifying the causal effect β^* . To illustrate the broad applicability of Condition 2a, we outline three representative scenarios below, considering a dimensionality of $p = 3$ for simplicity.

1. *Existence of Reference Environment.* Suppose that there exists a reference environment $e = 1$ without interventions, i.e. $\delta^{(1)} = 0$. In environment $e = 2$, the first two covariates are intervened with $\delta_1^{(2)}, \delta_2^{(2)} \neq 0$; while in environment $e = 3$, only the last covariate is intervened with $\delta_3^{(3)} \neq 0$. In this case, (12) is satisfied with $\mathcal{E}_1 = \{2, 3\}$ and $\mathcal{E}_2 = \{1\}$.
2. *Existence of Dominant Environment.* Suppose that there exists one environment e that is noisier than the other environment f , that is $\mathbb{E}[\delta^{(e)} \delta^{(e)\top}] \succ \mathbb{E}[\delta^{(f)} \delta^{(f)\top}]$ for some $e, f \in \mathcal{E}$. In this scenario, (12) holds if $\mathcal{E}_1 = \{e\}$, and $\mathcal{E}_2 = \{f\}$.
3. *Existence of Combined Dominating Environments.* Suppose that across environments $\mathcal{E} = \{1, 2, 3\}$, the interventions strength are as follows:

$$\mathbb{E}[\delta^{(1)} \delta^{(1)\top}] = \text{diag}(3, 3, 0), \quad \mathbb{E}[\delta^{(2)} \delta^{(2)\top}] = \text{diag}(0, 0, 3), \quad \mathbb{E}[\delta^{(3)} \delta^{(3)\top}] = \text{diag}(1, 1, 1).$$

Here, environments 1, 2, 3 have interventions on a subset of covariates but there does not exist one environment dominating others. However, the average of the first two environments dominates the third, that is, $\frac{1}{2} \mathbb{E}[\delta^{(1)} \delta^{(1)\top}] + \frac{1}{2} \mathbb{E}[\delta^{(2)} \delta^{(2)\top}] \succ \mathbb{E}[\delta^{(3)} \delta^{(3)\top}]$, thus satisfying (12).

We emphasize again that Condition 2a requires only the existence of two such collections of environments, without needing to identify or specify them exactly. The following theorem confirms that β^* is identifiable under Condition 2a in the additive intervention regime, and our proposed NegDRO approach, as formulated in (8), recovers β^* exactly.

Theorem 1. Suppose that Conditions 1 and 2a hold. The set of risk-invariant prediction models becomes a singleton of the causal effect β^* such that $\mathcal{B}_{\text{inv}}(\mathcal{E}) = \{\beta^*\}$. Consequently, our proposed b_{Neg}^∞ defined in (8) recovers β^* .

The implications in Theorem 1 are two-fold. Firstly, if there are two collections of environments such that the weighted average of interventions in one collection dominates the counterpart in the other collection (as specified in Condition 2a), the causal effect β^* becomes the only valid prediction model achieving **Invariance Principle**. Secondly, our proposed NegDRO identifies the causal effect β^* when the regularization parameter γ is set to ∞ , since b_{Neg}^∞ as defined in (8) enforces identical risk across environments.

Notably, Condition 2a offers concrete requirements on environmental heterogeneity for causal discovery. In existing literature, such sufficient environmental heterogeneity is often presumed and stated at a high level in the sense that the observed environments have already been diverse enough that selecting any non-direct causes of the outcome will violate the invariance principle, as seen in the Identification Condition of Fan et al. [2023] and the Effectiveness Assumption of Yin et al. [2024]. In contrast, our proposed Condition 2a establishes concrete conditions directly regarding the added interventions of observed environments, guiding the applied scientists to assess or even design heterogeneous environments for causal identification.

Next, we present an equivalent expression of Condition 2a, making it especially useful for subsequent theoretical analysis. For any $w \in \Delta^{|\mathcal{E}|}$, we define the matrix $\mathbf{A}(w) \in \mathbb{R}^{p \times p}$ as:

$$\mathbf{A}(w) = \sum_{e \in \mathcal{E}} \left(w_e - \frac{1}{|\mathcal{E}|} \right) \mathbb{E}[\delta^{(e)} \delta^{(e)\top}]. \quad (13)$$

The matrix $\mathbf{A}(w)$ quantifies the discrepancy between the w -weighted average of interventions across *all environments* and the simple average of interventions over *all environments*. The alternative causal identification condition based on $\mathbf{A}(w)$ is as follows:

Condition 2b. There exists some $w^0 \in \Delta^{|\mathcal{E}|}$ such that $\lambda = \lambda_{\min}(\mathbf{A}(w^0)) > 0$, where $\lambda_{\min}(\cdot)$ denotes the smallest eigenvalue of a matrix.

Condition 2b indicates the existence of a convex combination of environments' interventions that strictly dominates the simple average of interventions, such that $\sum_{e \in \mathcal{E}} w_e^0 \mathbb{E}[\delta^{(e)} \delta^{(e)\top}] \succ \sum_{e \in \mathcal{E}} \frac{1}{|\mathcal{E}|} \mathbb{E}[\delta^{(e)} \delta^{(e)\top}]$ for some unknown $w^0 \in \Delta^{|\mathcal{E}|}$. Furthermore, the magnitude of λ reflects the degree of heterogeneity among environments. A large λ implies a greater discrepancy between the w^0 -weighted average and the simple average of interventions, signaling more pronounced heterogeneity.

The following proposition establishes the equivalence between Conditions 2a and 2b:

Proposition 1. Conditions 2a and 2b are equivalent.

In the following discussions, we will focus on Condition 2b, as it provides a concise form for environmental heterogeneity via the matrix $\mathbf{A}(w^0)$, facilitating the development of theoretical results. With the equivalence established in Proposition 1, Condition 2b is sufficient for \mathcal{B}_{inv} uniquely identifying β^* , as demonstrated in Theorem 1. Essentially, Condition 2b is not only sufficient, but also nearly necessary, as shown in the following Theorem.

Theorem 2. Suppose Condition 1 holds, and the additive intervention affects at most one position in each environment, i.e. $|\text{supp}(\delta^{(e)})| \leq 1$ for all $e \in \mathcal{E}$. If $\mathcal{B}_{\text{inv}}(\mathcal{E}) = \{\beta^*\}$, then there must exist some $w^0 \in \Delta^{|\mathcal{E}|}$ satisfying that $\mathbf{A}(w^0) \succ 0$.

This theorem focuses on a specific pattern of additive interventions, where each environment $e \in \mathcal{E}$ intervenes at most one position of covariates' noises. For instance, in environment $e = 1$, if we only

intervene in the first position of the covariate, i.e., $X_1^{(1)}$, while others remain unaffected, then $[\delta^{(1)}]_{2:p} = 0$ and $\text{supp}(\delta^{(1)}) = \{1\}$. Within this context, Theorem 1 and 2 together suggest that Condition 2b is both sufficient and necessary for \mathcal{B}_{inv} uniquely identifying β^* . The following example illustrates the necessity of Condition 2b:

Example 3. Consider $X^{(e)} \in \mathbb{R}^3$, and let the additive interventions in environments $\mathcal{E} = \{1, 2, 3\}$ be:

$$\mathbb{E}[\delta^{(1)}\delta^{(1)\top}] = \text{diag}(1, 0, 0); \quad \mathbb{E}[\delta^{(2)}\delta^{(2)\top}] = \text{diag}(0, 1, 0); \quad \mathbb{E}[\delta^{(3)}\delta^{(3)\top}] = \text{diag}(0, 0, 1).$$

It is evident that Condition 2b is not satisfied in this case. In the Appendix, we demonstrate that there are multiple prediction models, including the causal effect β^* , achieving identical risks across environments. That is, $\beta^* \in \mathcal{B}_{\text{inv}}$ but $\mathcal{B}_{\text{inv}} \neq \{\beta^*\}$.

3.3 Causality Discovery with Finite γ

Thus far, we have established that Condition 2b is both sufficient and nearly necessary for ensuring that the set of risk invariant prediction models, \mathcal{B}_{inv} as defined in (4), uniquely identifies the causal effect β^* in the additive intervention regime. Under this identification condition, our proposed NegDRO exactly recovers the causal effect when the regularization parameter γ is set to ∞ . Next, we aim to analyze the behavior of NegDRO in the scenario with finite $\gamma \geq 0$, and demonstrate that b_{Neg}^γ , defined in (6), converges to β^* as γ increases to ∞ .

To facilitate the discussion, we introduce a transformation of $w \in \mathcal{U}(\gamma)$: $\tilde{w}_e = \frac{w_e + \gamma}{1 + \gamma|\mathcal{E}|}$ for each $e \in \mathcal{E}$. It is clear that $\sum_{e \in \mathcal{E}} \tilde{w}_e = 1$, and $\tilde{w}_e \geq 0$ for all $e \in \mathcal{E}$, implying that $\tilde{w} \in \Delta^{|\mathcal{E}|}$. We rewrite w_e as $w_e = (1 + \gamma|\mathcal{E}|)\tilde{w}_e - \gamma$ for each $e \in \mathcal{E}$. Using this transformation, the original minimax optimization for NegDRO in (6) is reformulated as:

$$b_{\text{Neg}}^\gamma = \arg \min_{b \in \mathbb{R}^p} \max_{w \in \Delta^{|\mathcal{E}|}} \sum_{e \in \mathcal{E}} (1 + \gamma|\mathcal{E}|)w_e - \gamma \mathbb{E}[\ell(X^{(e)}, Y^{(e)}; b)].$$

By dividing $1 + \gamma|\mathcal{E}|$, we obtain an equivalent representation for b_{Neg}^γ defined in (6),

$$b_{\text{Neg}}^\gamma = \arg \min_{b \in \mathbb{R}^p} \Phi(b), \quad \text{where} \quad \Phi(b) = \max_{w \in \Delta^{|\mathcal{E}|}} \sum_{e \in \mathcal{E}} \left(w_e - \frac{\gamma}{1 + \gamma|\mathcal{E}|} \right) \mathbb{E}[\ell(X^{(e)}, Y^{(e)}; b)]. \quad (14)$$

We establish the dependence of $\|b_{\text{Neg}}^\gamma - \beta^*\|_2$ on γ in the following Proposition.

Proposition 2. Suppose that Conditions 1 and 2b hold. Then, the global optimizer b_{Neg}^γ , defined in (14), satisfies

$$\|b_{\text{Neg}}^\gamma - \beta^*\|_2 \leq \frac{C\sigma_Y^2}{\lambda(1 + \gamma|\mathcal{E}|)}, \quad (15)$$

where $\lambda > 0$ is defined in Condition 2b, and $C > 0$ represents a positive constant.

This proposition indicates that optimizer b_{Neg}^γ of NegDRO problem is $\mathcal{O}((\gamma|\mathcal{E}|)^{-1})$ -close to the causal effect β^* . A few key insights emerge from this result. Firstly, as the regularization parameter γ increases, the distance between b_{Neg}^γ and β^* decreases, bringing b_{Neg}^γ closer to β^* . In the extreme case where $\gamma = \infty$, b_{Neg}^γ exactly matches β^* , consistent with the result in Theorem 1 that $b_{\text{Neg}}^\infty = \beta^*$. Secondly, with a higher degree of environmental heterogeneity and more observed environments, as λ and $|\mathcal{E}|$ being larger, the proposed NegDRO yields the optimizer closer to the causal effect β^* .

However, finding the global optimizer of the NegDRO problem, as defined in (14), is computationally challenging due to the nonconvexity of $\Phi(b)$ with respect to b . Notably, the combination weight in front of

each environment’s risk is possibly negative, making $\sum_{e \in \mathcal{E}} (w_e - \frac{\gamma}{1+\gamma|\mathcal{E}|}) \mathbb{E}[\ell(X^{(e)}, Y^{(e)}; b)]$ a potentially nonconvex function of b . Consequently, after maximizing over $w \in \Delta^{|\mathcal{E}|}$, the function $\Phi(b)$ remains a nonconvex function with respect to b . Classic optimization techniques, such as gradient descent and its variants (e.g., sub-gradient descent), may get trapped in local minima or saddle points due to the nonconvex landscape of $\Phi(b)$ [Boyd and Vandenberghe, 2004, Bonnans et al., 2006, Dauphin et al., 2014]. In the next Section 4, we establish that causal discovery is still achievable in a computationally efficient manner.

4 Computationally Efficient Causal Invariance Learning

We now turn to devising a computationally efficient algorithm for solving the NegDRO defined in (6). In the following Section 4.1, we introduce our key finding that any stationary point of NegDRO closely approximates the causal effect β^* , provided that the regularization parameter $\gamma > 0$ is sufficiently large. Building upon this finding, we design in Section 4.2 an efficient algorithm for estimating β^* , with the convergence rate established in terms of both sample size and iteration time.

4.1 Causal Discovery with Stationary Points

In this subsection, we demonstrate that any stationary point of NegDRO converges to the causal effect β^* with an increasing regularization parameter γ . The NegDRO objective $\Phi(b)$, as defined in (14), is not differentiable everywhere because the inner maximization $\max_{w \in \Delta^{|\mathcal{E}|}} \sum_{e \in \mathcal{E}} (w_e - \frac{\gamma}{1+\gamma|\mathcal{E}|}) \mathbb{E}[\ell(X^{(e)}, Y^{(e)}; b)]$ may have multiple solutions. To simplify the analysis and focus on the core insights, we add a ridge penalty on computing the optimal weights of the inner maximization such that the inner maximization has a unique solution and the objective function is differentiable. The full treatment of the original NegDRO, which involves the nonsmooth optimization problems, is provided later in Section 4.3.

Given a small $\mu > 0$, we define the penalized version of $\Phi(b)$ in (14) as follows:

$$\Phi_\mu(b) = \max_{w \in \Delta^{|\mathcal{E}|}} \left\{ \sum_{e \in \mathcal{E}} \left(w_e - \frac{\gamma}{1 + \gamma|\mathcal{E}|} \right) \mathbb{E}[\ell(X^{(e)}, Y^{(e)}; b)] - \mu \|w\|_2^2 \right\}. \quad (16)$$

Compared to the original $\Phi(b)$ in (14), where multiple weights may simultaneously maximize the objective, the penalized $\Phi_\mu(b)$ yields a unique maximizer weight for each b , as the objective becomes strongly concave with respect to w . For each prediction model $b \in \mathbb{R}^p$, we denote $\bar{w} = \bar{w}(b)$ as the unique maximizer weight satisfying:

$$\bar{w} := \arg \max_{w \in \Delta^{|\mathcal{E}|}} \sum_{e \in \mathcal{E}} \left\{ \left(w_e - \frac{\gamma}{1 + \gamma|\mathcal{E}|} \right) \mathbb{E}[\ell(X^{(e)}, Y^{(e)}; b)] - \mu \|w\|_2^2 \right\}. \quad (17)$$

By the Danskin’s theorem [Danskin, 1966][Bertsekas, 1997, Proposition B.25], $\Phi_\mu(b)$ is differentiable for every $b \in \mathbb{R}^p$, with the gradient defined as

$$\nabla \Phi_\mu(b) = \sum_{e \in \mathcal{E}} \left(\bar{w}_e - \frac{\gamma}{1 + \gamma|\mathcal{E}|} \right) \nabla \mathbb{E}[\ell(X^{(e)}, Y^{(e)}; b)].$$

In the following theorem, we shall leverage NegDRO’s gradient norm $\|\nabla \Phi_\mu(b)\|_2$ to control the distance between any prediction model b and the causal effect β^* .

Theorem 3. Suppose Conditions 1 and 2b hold. For a positive ridge-penalty parameter $\mu > 0$, the following inequality holds for any prediction model $b \in \mathbb{R}^p$:

$$\|b - \beta^*\|_2 \leq \frac{C}{\lambda} \left(\frac{\sigma_Y^2}{1 + \gamma|\mathcal{E}|} + \|\nabla \Phi_\mu(b)\|_2 \right) + C \sqrt{\frac{\mu}{\lambda}}, \quad (18)$$

where $\lambda > 0$ is defined in Condition 2b, and $C > 0$ stands for some universal constant.

This theorem indicates that the distance of $\|b - \beta^*\|_2$, for any prediction model $b \in \mathbb{R}^p$, is upper bounded via the gradient norm $\|\nabla\Phi_\mu(b)\|_2$, where $\Phi_\mu(b)$ is the penalized objective function defined in (16) associated with NegDRO. The inequality in (18) holds for any $\lambda > 0$, but for simplicity, we treat λ as a fixed constant, which is determined by the heterogeneity level across observed environments. The roles of the regularization parameter $\gamma \geq 0$ and the ridge-penalty parameter $\mu > 0$ are key to understanding this result. As γ increases, the first term, $\frac{\sigma_Y^2}{1+\gamma|\mathcal{E}|}$ diminishes to zero. Meanwhile, the choice of μ presents a tradeoff between $\|\nabla\Phi_\mu(b)\|_2$ and $\sqrt{\mu/\lambda}$. Specifically, while a smaller value of μ reduces $\sqrt{\mu/\lambda}$, it increases the number of iterations required for algorithms to locate a prediction model b with a sufficiently small $\|\nabla\Phi_\mu(b)\|_2$; see Proposition 3. In later Theorem 5, we provide guidance on choosing the optimal value of μ .

Now, we present the main idea for the proof of Theorem 3, which relies on the expression for the risk $\mathbb{E}[\ell(X^{(e)}, Y^{(e)}; b)]$, under the additive intervention regime specified in Condition 1:

$$\mathbb{E}[\ell(X^{(e)}, Y^{(e)}; b)] = \sigma_Y^2 + 2h^\top \mathbf{G}(b - \beta^*) + (b - \beta^*)^\top \mathbf{G}^\top \left(\mathbf{H} + \mathbb{E}[\delta^{(e)} \delta^{(e)\top}] \right) \mathbf{G}(b - \beta^*), \quad (19)$$

where the full-rank matrix $\mathbf{G} \in \mathbb{R}^{p \times p}$, the positive definite matrix $\mathbf{H} \succeq 0$ and the vector $h \in \mathbb{R}^p$ are defined in the Appendix. The risk expression (19) reveals that the first-order term involving $b - \beta^*$ remains invariant across environments, while the second-order terms vary with the interventions $\mathbb{E}[\delta^{(e)} \delta^{(e)\top}]$. The proof proceeds in three steps:

Step-1: Expressing $\Phi_\mu(b)$ through its gradient $\nabla\Phi_\mu(b)$. Given the quadratic nature of $\Phi_\mu(b)$ with respect to b , $\frac{1}{2}(b - \beta^*)^\top \nabla\Phi_\mu(b)$ matches $\Phi_\mu(b)$ in the second-order terms of b , differing only in the first-order and constant terms. After cancellation across environments, the summation of the constant and first-order terms of b scales by a factor of $\frac{1}{1+\gamma|\mathcal{E}|}$, yielding:

$$\Phi_\mu(b) = \frac{1}{2}(b - \beta^*)^\top \nabla\Phi_\mu(b) + \frac{1}{1+\gamma|\mathcal{E}|} [\sigma_Y^2 + h^\top \mathbf{G}(b - \beta^*)] - \mu \|\bar{w}\|_2^2.$$

Step-2: Establishing the lower bound of $\Phi_\mu(b)$. According to (17), $\Phi_\mu(b)$ is attained with the maximizer weight \bar{w} , and thus any other weight w^0 provides a lower bound for $\Phi_\mu(b)$.

$$\begin{aligned} \Phi_\mu(b) &\geq \sum_{e \in \mathcal{E}} (w_e^0 - \frac{\gamma}{1+\gamma|\mathcal{E}|}) \mathbb{E}[\ell(X^{(e)}, Y^{(e)}; b)] - \mu \|w^0\|_2^2 \\ &\geq \frac{1}{1+\gamma|\mathcal{E}|} [\sigma_Y^2 + 2h^\top \mathbf{G}(b - \beta^*)] + (b - \beta^*)^\top \mathbf{G}^\top \mathbf{A}(w^0) \mathbf{G}(b - \beta^*) - \mu \|w^0\|_2^2 \\ &\geq \frac{1}{1+\gamma|\mathcal{E}|} [\sigma_Y^2 + 2h^\top \mathbf{G}(b - \beta^*)] + \lambda \|\mathbf{G}(b - \beta^*)\|_2^2 - \mu \|w^0\|_2^2, \end{aligned}$$

where the second inequality uses the explicit risk expression (19) and $\mathbf{H} \succeq 0$, and the third inequality leverages Condition 2b to ensure $\mathbf{A}(w^0) \succeq \lambda \mathbf{I}$.

Step-3: Constructing the error bound using the gradient norm. Combining the above two steps, and applying Chebyshev's inequality, we obtain

$$\lambda \|\mathbf{G}(b - \beta^*)\|_2^2 \leq \left(\frac{1}{2} \|\nabla\Phi_\mu(b)\|_2 + \frac{\|h\|_2 \|\mathbf{G}\|_2}{1+\gamma|\mathcal{E}|} \right) \|b - \beta^*\|_2 + \mu (\|w^0\|_2^2 - \|\bar{w}\|_2^2).$$

Since $\|h\|_2 \leq c_1 \sigma_Y^2$, $\|\mathbf{G}\|_2 \leq c_2$, and $\|\mathbf{G}(b - \beta^*)\|_2 \geq c_3 \|b - \beta^*\|_2$, with $c_1, c_2, c_3 \geq 0$ standing for some universal constants, together with the fact that $\|w^0\|_2^2 - \|\bar{w}\|_2^2 \leq 1$, the desired result in Theorem 3 follows.

Next, we move from the population regime to the finite-sample regime, where observed data samples $\{x_i^{(e)}, y_i^{(e)}\}_{i=1}^{n_e}$ are drawn i.i.d from the distribution of $(X^{(e)}, Y^{(e)})$ for each environment $e \in \mathcal{E}$. Let $n = \min_{e \in \mathcal{E}} n_e$ denote the smallest sample size across all environments. We substitute the population risk $\mathbb{E}[\ell(X^{(e)}, Y^{(e)}; b)]$ in (14) with its empirical counterpart

$$\widehat{\mathbb{E}}[\ell(X^{(e)}, Y^{(e)}; b)] = \frac{1}{n_e} \sum_{i=1}^{n_e} \ell(x_i^{(e)}, y_i^{(e)}; b),$$

resulting in the empirical penalized NegDRO problem:

$$\min_{b \in \mathbb{R}^p} \widehat{\Phi}_\mu(b), \quad \text{with} \quad \widehat{\Phi}_\mu(b) = \max_{w \in \Delta^{|\mathcal{E}|}} \sum_{e \in \mathcal{E}} \left\{ \left(w_e - \frac{\gamma}{1 + \gamma|\mathcal{E}|} \right) \widehat{\mathbb{E}}[\ell(X^{(e)}, Y^{(e)}; b)] - \mu \|w\|_2^2 \right\}. \quad (20)$$

The analysis of the empirical optimization problem typically requires the tail assumptions of the noise distributions, such as those in [Rothenhäusler et al. \[2019\]](#), [Fan et al. \[2023\]](#). We assume the noise to be sub-Gaussian in the following condition.

Condition 3. $\eta \in \mathbb{R}^{p+1}$ and $\delta^{(e)} \in \mathbb{R}^p$ for all $e \in \mathcal{E}$ in (9) are sub-Gaussian random vectors.

The following theorem establishes a finite-sample bound for the distance between any prediction model $b \in \mathbb{R}^p$ and the causal effect β^* .

Theorem 4. Suppose Conditions 1, 2b, and 3 hold, and the sample size satisfies $n \geq 2p(\frac{c}{\lambda^2} \vee 1)$, for some constant $c > 0$. For a ridge-penalty parameter $\mu > 0$, the following inequality holds for any prediction model $b \in \mathbb{R}^p$: with probability at least $1 - 2|\mathcal{E}|e^{-s}$,

$$\|b - \beta^*\|_2 \leq \frac{C}{\lambda} \left(\frac{\sigma_Y^2}{1 + \gamma|\mathcal{E}|} + \|\nabla \widehat{\Phi}_\mu(b)\|_2 \right) + \frac{C}{\sqrt{\lambda}} \left[\sqrt{\mu} + \left(\frac{p+s}{n} \right)^{1/4} \right], \quad (21)$$

for any $s \in (0, (\frac{\lambda^2}{c} \wedge 1)n]$, where $\lambda > 0$ is defined in Condition 2b, and $C > 0$ stands for some constant.

Compared to the population-level result established in Theorem 3, the roles of the regularization parameter $\gamma \geq 0$ and the ridge-penalty $\mu > 0$ remain consistent. The only difference lies in the introduction of an additional finite-sample error term of order $\mathcal{O}(n^{-1/4})$ within the empirical upper bound in (21). In the subsequent Section 4.2, we present an algorithm to locate a stationary point of $\widehat{\Phi}_\mu(\cdot)$, ensuring that $\|\widehat{\Phi}_\mu(\cdot)\|_2$ approaches zero with a growing number of iterations. Essentially, the number of iterations required is inversely proportional to the magnitude of μ . To balance the computational cost of finding a prediction model with a small $\|\nabla \widehat{\Phi}_\mu(b)\|_2$ and the impact of $\sqrt{\mu/\lambda}$ on the bound of (21), we provide guidance on the optimal selection of μ in Theorem 5..

4.2 Searching for Stationary Points

We start with designing an algorithm to locate stationary points of $\widehat{\Phi}_\mu(\cdot)$ and then establish its convergence rate to β^* with respect to both sample size and iteration times. To identify a stationary point for the non-convex $\widehat{\Phi}_\mu(b)$, we propose a standard gradient descent Algorithm 1. In each iteration t , given the current b^t , the weight w^{t+1} is chosen to maximize the penalized objective as in (22). Since the objective is a strongly concave function towards w , we apply the Danskin's theorem to compute the gradient $\nabla \widehat{\Phi}_\mu(b^t)$ using the optimal weight w^{t+1} , as in (23).

To facilitate a theoretical analysis of Algorithm 1, we impose an additional assumption concerning the smoothness of the environment's risk function. This smoothness assumption is standard in the analysis of convergence for algorithms solving nonconvex optimization problems [[Ghadimi and Lan, 2013](#), [Kingma, 2014](#), [Lee et al., 2016](#)].

Condition 4 (Smoothness). For $e \in \mathcal{E}$, the empirical risk $\widehat{\mathbb{E}}[\ell(X^{(e)}, Y^{(e)}; b)] = \frac{1}{n_e} \sum_{i=1}^{n_e} \ell(x_i^{(e)}, y_i^{(e)}; b)$ is M -smooth with respect to $b \in \mathbb{R}^p$, that is, for any $b, b' \in \mathbb{R}^p$,

$$\left\| \nabla \widehat{\mathbb{E}}[\ell(X^{(e)}, Y^{(e)}; b)] - \nabla \widehat{\mathbb{E}}[\ell(X^{(e)}, Y^{(e)}; b')] \right\|_2 \leq M \|b - b'\|_2.$$

Algorithm 1: Gradient Descent Algorithm for the Penalized NegDRO in (20)

Input : Iteration time T , step sizes $\{\alpha^t\}_{t=0}^T$, initial point b^0 , regularization parameter $\gamma \geq 0$, ridge-penalty parameter $\mu > 0$

Output: \hat{b}^γ

for $t = 0, 1, \dots, T$ **do**

Update the optimal weight associated with b^t :

$$w^{t+1} = \arg \max_{w \in \Delta^{|\mathcal{E}|}} \left\{ \sum_{e \in \mathcal{E}} \left(w_e - \frac{\gamma}{1 + \gamma|\mathcal{E}|} \right) \widehat{\mathbb{E}}[\ell(X^{(e)}, Y^{(e)}; b^t)] - \mu \|w\|_2^2 \right\}; \quad (22)$$

Update b^{t+1} corresponding to the weight w^{t+1} :

$$b^{t+1} = b^t - \alpha^t \nabla \widehat{\Phi}_\mu(b^t), \quad \text{with } \nabla \widehat{\Phi}_\mu(b^t) = \sum_{e \in \mathcal{E}} \left(w_e^{t+1} - \frac{\gamma}{1 + \gamma|\mathcal{E}|} \right) \nabla \widehat{\mathbb{E}}[\ell(X^{(e)}, Y^{(e)}; b^t)]; \quad (23)$$

end

Define $\hat{b}^\gamma \in \arg \min_{\{b^t\}_{t=1}^T} \|\nabla \widehat{\Phi}_\mu(b^t)\|_2$.

We now establish the convergence rate of Algorithm 1's output to a stationary point of $\widehat{\Phi}_\mu(\cdot)$.

Proposition 3. Suppose Condition 4 holds. By setting the step size in Algorithm 1 as $\alpha^t = \frac{1}{2M+2M^2/\mu}$ for all $t = 0, \dots, T$, the output \hat{b}^γ of Algorithm 1 satisfies:

$$\|\nabla \widehat{\Phi}_\mu(\hat{b}^\gamma)\|_2 \leq \sqrt{\frac{1}{T} \sum_{t=1}^T \|\nabla \widehat{\Phi}_\mu(b^t)\|_2^2} \leq \sqrt{\frac{4(M + M^2/\mu) \widehat{\Phi}_\mu(b^0)}{T}},$$

where b^0 is the initial point in Algorithm 1, and M is the smoothness parameter defined in Condition 4.

The result aligns with similar findings on stationary convergence rates of gradient descent methods in the literature [Bottou et al., 2018]. Notably, this stationary convergence rate is optimal for first-order methods, as established by Carmon et al. [2020], Nesterov et al. [2018].

In the following theorem, we establish the convergence rate of $\|\hat{b}^\gamma - \beta^*\|_2$ by combining Theorem 4 and Proposition 3.

Theorem 5. Suppose Conditions 1, 2b, 3, 4 hold, and the sample size satisfies $n \geq 2p(\frac{c}{\lambda^2} \vee 1)$ for some constant $c > 0$. For a ridge-penalty parameter $\mu > 0$, by setting the step size in Algorithm 1 as $\alpha^t = \frac{1}{2M+2M^2/\mu}$ for all $t = 0, \dots, T$, then with probability at least $1 - 2|\mathcal{E}|e^{-s}$, the output \hat{b}^γ of Algorithm 1 satisfies

$$\|\hat{b}^\gamma - \beta^*\|_2 \leq \frac{C}{\lambda} \left(\frac{\sigma_Y^2}{1 + \gamma|\mathcal{E}|} + \sqrt{\frac{M + M^2/\mu}{T}} \right) + \frac{C}{\lambda^{1/2}} \left[\mu^{1/2} + \left(\frac{p+s}{n} \right)^{1/4} \right],$$

for any $s \in (0, (\frac{\lambda^2}{c} \wedge 1)n]$, where $\lambda > 0$ is defined in Condition 2b, M denotes the smoothness parameter defined in Condition 4, and $C > 0$ stands for some constant.

Notably, unlike existing methods that require an exhaustive search over all possible subsets of covariates, Algorithm 1 avoids the computational burden and remains efficient even with a large dimension p . In

Section 6, we present empirical results demonstrating its computational efficiency and effectiveness in causal discovery.

A few remarks are provided in order for Theorem 5. For a constant λ , when we set the penalty parameter $\mu = \frac{cM}{\sqrt{T}}$ for some constant $c > 0$, the bound in the preceding theorem is simplified as follows:

$$\|\hat{b}^\gamma - \beta^*\|_2 \lesssim \frac{\sigma_Y^2}{1 + \gamma|\mathcal{E}|} + \left(\frac{M^2}{T}\right)^{1/4} + \left(\frac{p}{n}\right)^{1/4}.$$

This result implies that Algorithm 1 produces an output \hat{b}^γ that approximates the causal effect β^* up to the level $\mathcal{O}((\gamma|\mathcal{E}|)^{-1} + T^{-1/4} + n^{-1/4})$. If we treat the count of environments $|\mathcal{E}|$ as constant, to achieve an ϵ -accurate solution, i.e. $\|\hat{b}^\gamma - \beta^*\|_2 \leq \epsilon$, it is sufficient to set the regularization parameter as $\gamma = \Omega(\epsilon^{-1})$, collect a sample size of $n = \Omega(\epsilon^{-4})$, and iterate Algorithm 1 for $T = \Omega(\epsilon^{-4})$ steps.

As demonstrated in Figure 7 in Section 6, our numerical studies demonstrate that our proposed NegDRO estimator achieves a convergence rate of $\mathcal{O}(n^{-1/4})$, indicating the tightness of our current analysis of \hat{b}^γ , the output of Algorithm 1. However, it remains an open question how to design a computationally efficient algorithm with an output achieving the convergence rate $\mathcal{O}(n^{-1/2})$, which deserves future investigation.

A natural question arises regarding the optimization convergence rate: can the convergence rate of $\|\hat{b}^\gamma - \beta^*\|_2$ with respect to iteration times T be further improved? The derived convergence rate for $\|\hat{b}^\gamma - \beta^*\|_2$ is obtained by combining the stationary point convergence result $\|\widehat{\Phi}_\mu(\hat{b}^\gamma)\|_2$ from Proposition 3, together with the upper bound on $\|b - \beta^*\|$ for any prediction model $b \in \mathbb{R}^p$ as established in Theorem 3. From the stationary point convergence perspective, the optimal rate for smooth functions is known to be $\mathcal{O}(T^{-1/2})$, as shown in Proposition 3. However, tuning the ridge penalty to ensure smoothness slows the rate to $\mathcal{O}(T^{-1/4})$ as shown in Theorem 5. Without imposing additional structural assumptions, these stationary convergence rates are considered optimal within the framework of optimization theory. Nonetheless, it may be possible to improve the convergence rate for $\|\hat{b}^\gamma - \beta^*\|_2$ by directly establishing point convergence using other problem structures that remain unidentified in this work, rather than relying on stationary convergence. We highlight that existing nonconvex landscape conditions [Karimi et al., 2016], such as the PL condition, might not hold for NegDRO problems with a finite γ as the true causal relationship β^* might not be an optimal solution to such NegDRO problems. Thus, none of the existing lower bounds would apply. We leave the investigation on the tightness of the convergence rate for future studies.

4.3 NegDRO without the Ridge Penalty

In this subsection, we extend our analysis to the original empirical NegDRO problem, without the ridge penalty used in previous discussions, defined as follows:

$$\min_{b \in \mathbb{R}^p} \widehat{\Phi}(b), \quad \text{with} \quad \widehat{\Phi}(b) = \max_{w \in \Delta^{|\mathcal{E}|}} \sum_{e \in \mathcal{E}} \left\{ \left(w_e - \frac{\gamma}{1 + \gamma|\mathcal{E}|} \right) \widehat{\mathbb{E}}[\ell(X^{(e)}, Y^{(e)}; b)] \right\}. \quad (24)$$

While most results remain consistent with the results in Sections 4.1 and 4.2, the current section requires a more general definition of stationary points due to the nonsmooth nature of $\widehat{\Phi}(b)$. To facilitate discussions, we introduce the concepts of Goldstein subdifferential and generalized stationary points.

Definition 3 (Goldstein Subgradient and Subdifferential). Given a function $h : \mathbb{R}^p \rightarrow \mathbb{R} \cup \{\infty\}$, a vector $\zeta \in \mathbb{R}^p$ is called a subgradient of h at a point $b \in \mathbb{R}^p$ if it satisfies:

$$h(b') \geq h(b) + \zeta^\top(b' - b) + o(\|b' - b\|_2), \quad \text{for all } b' \text{ such that } b' \rightarrow b.$$

The subdifferential of h at b , denoted as $\partial h(b)$, is the set of all subgradients at b :

$$\partial h(b) = \left\{ \zeta \in \mathbb{R}^p \mid h(b') \geq h(b) + \zeta^\top(b' - b) + o(\|b' - b\|_2), \text{ for all } b' \text{ such that } b' \rightarrow b \right\}.$$

The distance of subdifferential $\partial h(b)$ to the origin is given by $\text{Dist}(0, \partial h(b)) = \inf\{\|\zeta\|_2, \zeta \in \partial h(b)\}$.

In the following, unless otherwise specified, the terms ‘‘subgradient’’ and ‘‘subdifferential’’ refer to the Goldstein subgradient and Goldstein subdifferential, respectively. The subdifferential generalizes the notation of gradient. If the function $h(\cdot)$ is differentiable at the point b , the subdifferential reduces to its gradient with $\partial h(b) = \{\nabla h(b)\}$, and its distance to the origin becomes the gradient norm such that $\text{Dist}(0, \partial h(b)) = \|\nabla h(b)\|_2$. Building upon the definition of subdifferential, we define generalized stationary points as follows.

Definition 4 (Stationary Point). A point $b \in \mathbb{R}^p$ is a stationary point of the function $h : \mathbb{R}^p \rightarrow \mathbb{R} \cup \{\infty\}$ if and only if $0 \in \partial h(b)$, that is, $\text{Dist}(0, \partial h(b)) = 0$.

It extends the classic definition of stationary point utilized for differentiable functions, where a point b is a stationary point of the differentiable function $h(\cdot)$ if and only if $\|\nabla h(b)\|_2 = 0$.

As a generalization of Theorem 4, the following theorem establishes the distance $\|b - \beta^*\|_2$ in terms of the subdifferential $\partial \widehat{\Phi}(b)$.

Theorem 6. Suppose Conditions 1, 2b, 3 hold, and the sample size satisfies $n \geq 2p(\frac{c}{\lambda^2} \vee 1)$ for some constant $c > 0$. The following holds for any prediction model $b \in \mathbb{R}^p$: with probability at least $1 - 2|\mathcal{E}|e^{-s}$,

$$\|b - \beta^*\|_2 \leq \frac{C}{\lambda} \left(\frac{\sigma_Y^2}{1 + \gamma|\mathcal{E}|} + \text{Dist}(0, \partial \widehat{\Phi}(b)) \right) + \frac{C}{\lambda^{1/2}} \left(\frac{p+s}{n} \right)^{1/4}, \quad (25)$$

for any $s \in (0, (\frac{\lambda^2}{c} \wedge 1)n]$, where $\text{Dist}(0, \partial \widehat{\Phi}(b)) = \inf\{\|\zeta\|_2, \zeta \in \partial \widehat{\Phi}(b)\}$ measures the distance of the subdifferential $\partial \widehat{\Phi}(b)$ to the origin, $\lambda > 0$ is defined in Condition 2b, and $C > 0$ stands for some constant.

This bound closely aligns with the penalized case in Theorem 4, except for two differences: the gradient norm is replaced with the subdifferential distance, and the term related to the ridge-penalty parameter μ is removed. Moreover, this theorem implies that if b is a stationary point of $\widehat{\Phi}(\cdot)$ satisfying $\text{Dist}(0, \partial \widehat{\Phi}(b)) = 0$, it closely approximates the causal effect β^* with an error $\|b - \beta^*\|_2 = \mathcal{O}((\gamma|\mathcal{E}|)^{-1} + n^{-1/4})$, consistent with the results for the penalized case in Theorem 4.

To compute stationary points of the nonsmooth function $\widehat{\Phi}(b)$, we introduce a subgradient-based Algorithm 2, which updates the prediction model b^t using subgradient descent and employs a proximal mapping to facilitate convergence. The proximal mapping, defined for a parameter $v > 0$, is given by:

$$\text{prox}_{v\widehat{\Phi}}(b) = \arg \min_{\zeta \in \mathbb{R}^p} \left\{ \widehat{\Phi}(\zeta) + \frac{1}{2v} \|\zeta - b\|_2^2 \right\}. \quad (26)$$

We now comment on the subtle difference in the last output selection step between the current Algorithm 2 and the earlier Algorithm 1. For the ridge-penalized NegDRO which is differentiable, Algorithm 1 selects the output by minimizing the gradient norm $\|\nabla \widehat{\Phi}_\mu(b^t)\|_2$. This ensures the selected \hat{b}^γ approaches a stationary point of smooth $\widehat{\Phi}_\mu(\cdot)$ with a nearly zero $\|\nabla \widehat{\Phi}_\mu(b^\gamma)\|_2$. In contrast, for the unpenalized NegDRO which is not differentiable everywhere, the subdifferential distances to the origin, $\text{Dist}(0, \partial \widehat{\Phi}(b^t))$ for $t = 1, \dots, T$, are not directly observable. To address this issue, the current Algorithm 2 employs the proximal mapping to ensure that the subdifferential distance to the origin, $\text{Dist}(0, \partial \widehat{\Phi}(b^\gamma))$, is close to zero, thereby effectively approaching a stationary point for the nonsmooth $\widehat{\Phi}(\cdot)$. A detailed analysis is provided in the Appendix.

Now, we analyze the output of Algorithm 2 by establishing its convergence rate towards the causal effect β^* .

Algorithm 2: Subgradient Descent Algorithm for NegDRO in (24)

Input : Iteration time T , step sizes $\{\alpha^t\}_{t=0}^T$, initial point b^0 , regularization parameter $\gamma \geq 0$, proximal-mapping parameter $v > 0$

Output: \hat{b}^γ

for $t = 0, 1, \dots, T$ **do**

 Update the optimal weight w^{t+1} associated with b^t :

$$w^{t+1} \in \arg \max_{w \in \Delta^{|\mathcal{E}|}} \sum_{e \in \mathcal{E}} \left(w_e - \frac{\gamma}{1 + \gamma|\mathcal{E}|} \right) \widehat{\mathbb{E}}[\ell(X^{(e)}, Y^{(e)}; b^t)].$$

 Update b^{t+1} corresponding to the weight w^{t+1} :

$$b^{t+1} = b^t - \alpha^t \cdot \left\{ \sum_{e \in \mathcal{E}} \left(w_e^{t+1} - \frac{\gamma}{1 + \gamma|\mathcal{E}|} \right) \nabla \widehat{\mathbb{E}}[\ell(X^{(e)}, Y^{(e)}; b^t)] \right\}$$

 Compute proximal mapping point $\text{prox}_{v\widehat{\Phi}}(b^{t+1})$ as in (26).

end

Define $\hat{b}^\gamma \in \arg \min_{\{b^t\}_{t=1}^T} \|\text{prox}_{v\widehat{\Phi}}(b^t) - b^t\|_2$.

Theorem 7. Suppose Conditions 1, 2b, 3, 4 hold, and the sample size satisfies $n \geq 2p(\frac{c_1}{\lambda^2} \vee 1)$, for some constant $c_1 > 0$. By setting the proximal mapping parameter $v \in (0, c_2]$ and the step size as $\alpha^t = \frac{c_3}{\sqrt{T+1}}$ for all $t = 0, \dots, T$, for some constants $c_2, c_3 > 0$, with probability at least $1 - 2|\mathcal{E}|e^{-s}$, the output \hat{b}^γ of Algorithm 2 satisfies:

$$\|\hat{b}^\gamma - \beta^*\|_2 \leq \frac{C}{\lambda} \left(\frac{\sigma_Y^2}{1 + \gamma|\mathcal{E}|} + \left(\frac{1}{T} \right)^{1/4} \right) + \frac{C}{\lambda^{1/2}} \left(\frac{p+s}{n} \right)^{1/4},$$

for any $s \in (0, (\frac{\lambda^2}{c_1} \wedge 1)n]$, where λ is defined in Condition 2b, and $C > 0$ stands for a universal constant.

The above theorem shows that the output \hat{b}^γ approximates β^* up to an error $\mathcal{O}((\gamma|\mathcal{E}|)^{-1} + T^{-1/4} + n^{-1/4})$, aligned with the penalized case in Theorem 5 when the ridge-penalty parameter μ is set to cM/\sqrt{T} . The convergence rates with respect to both the sample size n and iteration times T are consistent with those discussed for Theorem 5. Notably, finding generalized stationary points for non-smooth functions, such as our NegDRO objective $\widehat{\Phi}(b)$, inherently requires a $T^{-1/4}$ convergence rate [Davis and Drusvyatskiy, 2018]. This aligns with the optimization convergence rate obtained when smoothing is applied and the ridge penalty is tuned appropriately, as in the penalized case Theorem 5.

5 Minimization Helps

In this section, we explore scenarios where interventions are limited—only a subset of covariates are intervened upon, which frequently happens in practice due to the cost or ethical constraints [Cohen et al., 2008, Brannath et al., 2009, Banerjee and Duflo, 2009]. These limited intervention settings introduce an additional challenge for causal discovery: multiple prediction models, including β^* , may yield invariant risks across environments. Despite this, NegDRO still has the potential of identifying β^* , due to the additional minimization step embedded in the NegDRO formulation in (8).

In Section 5.1, we introduce the identification Condition 6 which allows NegDRO to identify β^* in limited intervention settings. Building on this, Section 5.2 highlights the advantages of NegDRO in such limited

intervention settings, particularly when compared to other causal invariance learning methods designed for the additive intervention [Rothenhäusler et al., 2019, Shen et al., 2023].

5.1 Causal Identification under Limited Interventions

We illustrate causal discovery in the limited intervention regime by considering an important setting as described in the following Condition 5 and present a more general result in the Appendix. To formalize this scenario, we define $D \subset [p]$ as the set of covariates that are direct children of the outcome, with $D = \text{supp}(\mathbf{B}_{YX})$. Here, \mathbf{B}_{YX} captures the reverse effect of the outcome on the covariates, as defined in (9). The complement $D^c = [p] \setminus D$ corresponds to covariates that are not directly affected by the outcome. We impose the following specific condition to define this scenario:

Condition 5 (Additive Intervention with No Hidden Confounding and Separated Intervention). The additive intervention Condition 1 holds with $\eta = (\eta_X, \eta_Y)^\top \in \mathbb{R}^{p+1}$ and $\delta^{(e)} \in \mathbb{R}^p$ satisfying:

$$\mathbb{E}[\eta_Y \eta_X] = 0, \text{ and } \mathbb{E}[\delta_D^{(e)} \delta_{D^c}^{(e)}] = 0, \quad \forall e \in \mathcal{E}. \quad (27)$$

This condition imposes two additional assumptions within the additive intervention regime:

- *No Hidden Confounding.* The systematic random error η satisfies $\mathbb{E}[\eta_Y \eta_X] = 0$, implying $\mathbb{E}[\varepsilon_Y^{(e)} \varepsilon_X^{(e)}] = 0$, by the error decomposition model in (10). This aligns with no hidden confounding assumptions adopted in prior works [Hauser and Bühlmann, 2015, Peters et al., 2016, Ghassami et al., 2017].
- *Separated Interventions.* The environment-specific intervention $\delta^{(e)}$ satisfies $\mathbb{E}[\delta_D^{(e)} \delta_{D^c}^{(e)}] = 0$, for $e \in \mathcal{E}$. This indicates that the interventions applied to the direct children of the outcome $X_D^{(e)}$ and the remaining covariates $X_{D^c}^{(e)}$ are not correlated. This assumption is naturally satisfied in settings where interventions target only one covariate per environment or when independent interventions are applied to all covariates, for example, $\delta^{(e)} \sim \mathcal{N}(0, \Sigma^{(e)})$, where $\Sigma^{(e)}$ is a diagonal matrix.

Tailored for this setting, we propose the following identification condition:

Condition 6. Suppose there exists some weight $w^0 \in \Delta^{|\mathcal{E}|}$ satisfying $\sum_{e \in \mathcal{E}} w^0 \mathbb{E}[\varepsilon_X^{(e)} (\varepsilon_X^{(e)})^\top] \succ 0$, and

$$\mathbf{A}(w^0) \succeq 0, \quad [\mathbf{A}(w^0)]_{D,D} \succ 0, \quad (28)$$

where $\varepsilon_X^{(e)}$ represents the error used in (9), and $\mathbf{A}(\cdot)$ is defined in (13).

This identification condition serves as a relaxation of the earlier Condition 2b, by accommodating the limited intervention scenarios where only a subset of covariates are intervened upon, rather than the full set of covariates. The first requirement, $\sum_{e \in \mathcal{E}} w^0 \mathbb{E}[\varepsilon_X^{(e)} (\varepsilon_X^{(e)})^\top] \succ 0$, is automatically satisfied if the systematic random error η satisfies $\mathbb{E}[\eta \eta^\top] \succ 0$. The key difference emerges in the requirement on the matrix $\mathbf{A}(w^0)$ in (6). While the earlier Condition 2b requires $\mathbf{A}(w^0) \succ 0$ across all covariates, the current one requires only $[\mathbf{A}(w^0)]_{D,D}$, to be strictly positive, that is, the direct children of Y are sufficiently intervened. This means that under the new condition, the covariates outside D can remain unintervened across all environments, that is, $\delta_k^{(e)} = 0$ for some $k \notin D$ across all $e \in \mathcal{E}$.

To better illustrate this key relaxation, consider a thought experiment where researchers start with a reference environment with no interventions and then conduct a series of single-covariate interventions for each environment. For simplicity, we consider there are three covariates $p = 3$, and X_2 is the only direct child of the outcome Y , i.e., $D = \{2\}$. As demonstrated in Figure 3, Condition 6 requires intervening on the variable X_2 while Condition 2b requires intervening on all variables X_1, X_2 and X_3 .

Now we demonstrate that NegDRO identifies β^* under the relaxed condition in the setting described in Condition 5.

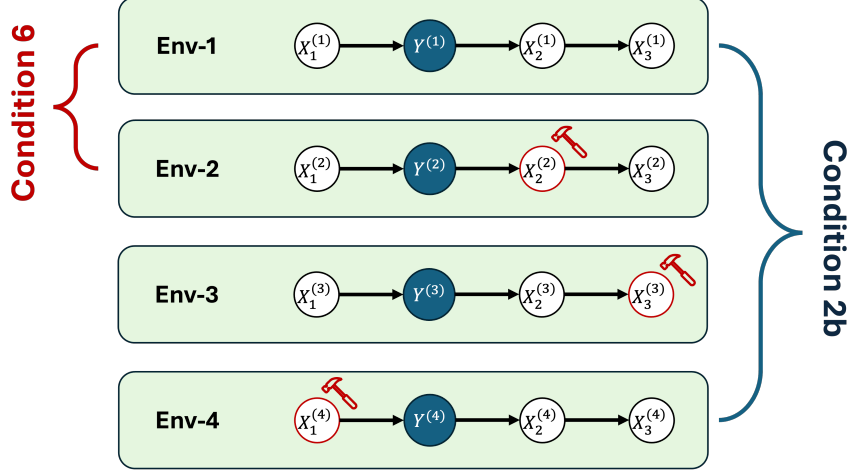


Figure 3: Comparison of Conditions 6 and 2b. Condition 6 requires intervening on the outcome's direct child (X_2) while Condition 2b requires intervening on all covariates (X_1, X_2, X_3).

Theorem 8. Suppose Conditions 5 and 6 hold. The proposed b_{Neg}^∞ , as defined as (8), identifies the causal effect with $b_{\text{Neg}}^\infty = \beta^*$.

Compared to Theorem 1, the above theorem enables the causal identification via the additional minimization step embedded in the NegDRO formulation in (8). Previously, in Theorem 1, the condition $\mathcal{A}(w^0) \succ 0$ ensures that β^* is the only prediction model satisfying risk invariance across environments. Consequently, since b_{Neg}^∞ is enforced to yield identical risks across environments, b_{Neg}^∞ aligns with β^* . However, under the limited intervention scenarios where some covariates remain unintervened across all environments, Condition 2b no longer holds and there may exist other invariant prediction models that are different from β^* . If these limited intervention scenarios satisfy the relaxed identification Condition 6, the additional minimization step in (8) effectively distinguishes β^* from other risk-invariant prediction models, ensuring the identification of β^* even when there exist multiple invariant prediction models.

Next, we analyze the output of Algorithm 2 by establishing its convergence rate towards the causal effect β^* under the relaxed identification Condition 6 in the regime described by Condition 5.

Theorem 9. Suppose Conditions 3, 4, 5 and 6 hold, and the sample size n satisfies $n \gg \gamma^2 p$. By setting the proximal-mapping parameter $v \in (0, c_1]$ and the step size as $\alpha^t = \frac{c_2}{\sqrt{T+1}}$ in Algorithm 2 for all $t = 0, \dots, T$, for some constants $c_1, c_2 > 0$, with probability at least $1 - 2|\mathcal{E}|e^{-s}$, the output \hat{b}^γ of Algorithm 2 satisfies:

$$\|\hat{b}^\gamma - \beta^*\|_2 \leq C\sigma_Y^2 \left\{ \frac{\gamma|\mathcal{E}|}{T^{1/4}} + \frac{(\gamma|\mathcal{E}|)^{1/4}}{T^{1/8}} + \frac{1}{(\gamma|\mathcal{E}|)^{1/4}} + \left(\frac{p+s}{n}\right)^{1/8} \right\},$$

for any $s \in (0, \frac{n}{\gamma^2})$, where $C > 0$ is a universal constant.

This theorem demonstrates that Algorithm 2 achieves causal discovery under the more relaxed causal identification Condition 6. Specifically, $\hat{b}^\gamma \rightarrow \beta^*$ as the regularization parameter γ , sample size n , and iteration time T become sufficiently large, satisfying $\gamma \rightarrow \infty$, $n \gg \gamma^2 p$, and $T \gg (\gamma|\mathcal{E}|)^4$. For $T = \Omega((\gamma|\mathcal{E}|)^5)$, the distance $\|\hat{b}^\gamma - \beta^*\|_2$ attains the rate $\mathcal{O}((\gamma|\mathcal{E}|)^{-1/4} + n^{-1/8})$. Compared to the upper bound established in Theorem 7, which relies on the stronger causal identification Condition 2b, the current upper bound requires larger values for γ and n , as well as a longer iteration time T , to achieve the same level of accuracy. Specifically, for an ϵ -accurate solution, i.e. $\|\hat{b}^\gamma - \beta^*\|_2 \leq \epsilon$, the required parameter values are $\gamma = \Omega(\epsilon^{-4})$, $n \gg \epsilon^{-8}$, and $T = \Omega(\epsilon^{-20})$, assuming the number of environments $|\mathcal{E}|$ and the covariate

dimension p are constants. It is worth noting that the current finite-sample rate of $n^{-1/8}$ and the optimization iteration complexity $T = \Omega(\epsilon^{-20})$ may not be optimal. Establishing the optimal convergence rate for this nonconvex problem is an intriguing question that we leave for future investigation.

5.2 Comparison to Gradient Matching Methods

We now compare NegDRO with existing approaches for additive interventions, specifically CausalDantzig [Rothenhäusler et al., 2019] and DRIG [Shen et al., 2023], in scenarios with limited interventions. We shall demonstrate that both CausalDantzig and DRIG are inapplicable to the limited intervention regime due to the fact that their key assumptions are violated in such a regime. In the following, we briefly introduce both methods and provide detailed introductions in the Appendix for completeness. CausalDantzig leverages the gradient invariance property inherent to additive interventions, formalized in its Proposition 1. This property states that for any pair of environments $e, f \in \mathcal{E}$, the causal effect β^* satisfies:

$$\mathbb{E}[X^{(e)}(Y^{(e)} - (\beta^*)^\top X^{(e)})] = \mathbb{E}[X^{(f)}(Y^{(f)} - (\beta^*)^\top X^{(f)})]. \quad (\text{Grad Invariance})$$

By assuming the non-singularity of $\mathbb{E}[X^{(e)}X^{(e)\top} - X^{(f)}X^{(f)\top}]$, CausalDantzig identifies β^* through:

$$\beta^* = \left(\mathbb{E}[X^{(e)}X^{(e)\top} - X^{(f)}X^{(f)\top}] \right)^{-1} \mathbb{E}[X^{(e)}Y^{(e)} - X^{(f)}Y^{(f)}].$$

However, this method fails under limited intervention scenarios. For example, suppose k -th covariate is not intervened upon across all environments, i.e., $\delta_k^{(e)} = 0$ for all $e \in \mathcal{E}$ for some $k \in [p]$. Then according to the SEMs in (11) and noise decomposition in (10), the difference of Gram matrices becomes

$$\mathbb{E}[X^{(e)}X^{(e)\top} - X^{(f)}X^{(f)\top}] = [(\mathbf{I} - \mathbf{B})^{-1}]_{-1,-1} \mathbb{E}[\delta^{(e)}\delta^{(e)\top} - \delta^{(f)}\delta^{(f)\top}] [(\mathbf{I} - \mathbf{B})^{-1}]_{-1,-1}^\top. \quad (29)$$

Here, the absence of interventions on $\delta_k^{(e)}$, for all $e \in \mathcal{E}$, renders $\mathbb{E}[\delta^{(e)}\delta^{(e)\top} - \delta^{(f)}\delta^{(f)\top}]$ and $\mathbb{E}[X^{(e)}X^{(e)\top} - X^{(f)}X^{(f)\top}]$ rank-deficient, violating the non-singularity assumption required for CausalDantzig. In contrast, our NegDRO approach remains effective to identify β^* under such limited intervention scenarios, provided that the identification Condition 6 is satisfied.

Now, we turn to discuss DRIG, which relies on the existence and availability of a *reference environment*, denoted as $e = 0$. This reference environment is characterized by strictly weaker interventions compared to all other environments $\mathcal{E} = \{1, 2, \dots, |\mathcal{E}|\}$ such that $\mathbb{E}[\delta^{(0)}\delta^{(0)\top}] \prec \mathbb{E}[\delta^{(e)}\delta^{(e)\top}]$ for all $e \in \mathcal{E}$. Given a regularization parameter $\gamma \geq 0$: DRIG solves the following optimization problem:

$$b_{\text{DRIG}}^\gamma = \arg \min_{b \in \mathbb{R}^p} \left\{ \mathbb{E}[\ell(X^{(0)}, Y^{(0)}; b)] + \gamma \sum_{e \in \mathcal{E}} w^e \left(\mathbb{E}[\ell(X^{(e)}, Y^{(e)}; b)] - \mathbb{E}[\ell(X^{(0)}, Y^{(0)}; b)] \right) \right\}, \quad (30)$$

where $w \in \Delta^{|\mathcal{E}|}$ is a pre-specified weight vector. While the primary focus of DRIG is to ensure robust generalization to unseen populations for finite γ , the method can achieve causal discovery with $b_{\text{DRIG}}^\infty = \beta^*$ when γ is set as ∞ , provided the reference environment $e = 0$ exists.

We emphasize that the reference environment plays a critical role in DRIG's formulation. With access to such an environment $e = 0$, it holds that $\mathbb{E}[X^{(e)}(X^{(e)})^\top] - \mathbb{E}[X^{(0)}(X^{(0)})^\top] \succ 0$ for all $e \in \mathcal{E}$. Consequently, the optimization problem in (30) becomes convex, since its Hessian $\mathbb{E}[X^{(0)}(X^{(0)})^\top] + \gamma \sum_{e \in \mathcal{E}} w^e (\mathbb{E}[X^{(e)}(X^{(e)})^\top] - \mathbb{E}[X^{(0)}(X^{(0)})^\top]) \succ 0$. This convexity significantly simplifies the computational effort, as DRIG requires solving only a convex optimization problem. This is a key distinction from our proposed NegDRO, which involves solving a nonconvex optimization problem without assuming the existence of a reference environment. However, it is challenging to identify a reference environment in

practice, limiting the application of the DRIG method. Moreover, under the limited intervention regime where some covariates are not intervened, such a reference environment does not exist. As an example, if $\delta_k^{(e)} = 0$ for all $e \in \mathcal{E}$ and for some $k \in [p]$, then $\mathbb{E}[\delta^{(e)}\delta^{(e)\top}] \not\sim \mathbb{E}[\delta^{(f)}\delta^{(f)\top}]$ for any pair $e, f \in \mathcal{E}$.

Next, we revisit Example 2 to compare the performance of NegDRO with CausalDantzig and DRIG under different intervention scenarios, including limited, weak, and full interventions.

Example 2 (Continued). Among the four covariates, $X_3^{(e)}$ is the only direct child of $Y^{(e)}$, i.e. $D = \{3\}$. We consider two environments with $\mathcal{E} = \{1, 2\}$. For each environment $e \in \mathcal{E}$, the noises $(\varepsilon_Y^{(e)}, \varepsilon_{1:4}^{(e)})^\top$ follow the distribution $(\varepsilon_Y^{(e)}, \varepsilon_{1:4}^{(e)})^\top \stackrel{d}{=} \eta + \begin{pmatrix} 0 \\ \delta^{(e)} \end{pmatrix}$, where the systematic random error $\eta \sim \mathcal{N}(0_4, \mathbf{I}_4)$. For environment $e = 1$, no interventions are applied to any covariates, so $\delta^{(1)} = 0_4$. For environment $e = 2$, the direct child $X_D^{(2)}$ is intervened such that $\delta_D^{(2)} \sim \mathcal{N}(0, 2)$. For the remaining covariates $X_{D^c}^{(2)}$, we examine the following intervention scenarios, which are illustrated in Figure 4.

(limited) $\delta_{D^c}^{(2)} = 0_3$; (weak) $\delta_{D^c}^{(2)} \stackrel{i.i.d.}{\sim} \mathcal{N}(0, 0.01)$; (strong) $\delta_{D^c}^{(2)} \stackrel{i.i.d.}{\sim} \mathcal{N}(0, 0.25)$.

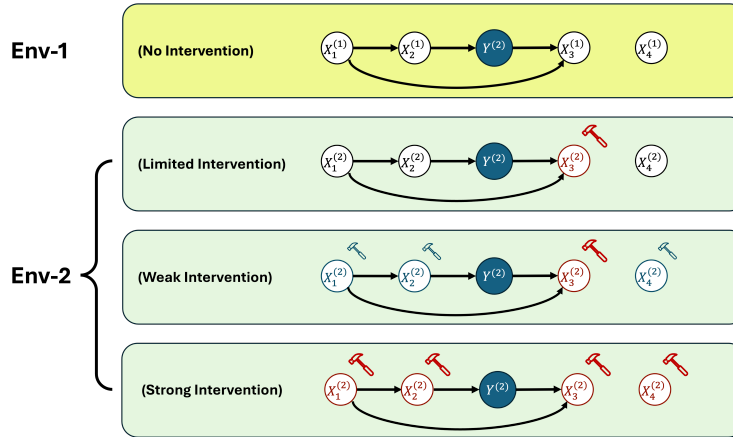


Figure 4: Illustration of Example 2. In environment $e = 1$, no interventions are applied, while environment $e = 2$ features three types of interventions. Red hammers denote “strong” interventions applied to a variable, blue hammers indicate “weak” interventions, and variables without hammers are not intervened.

Across the three intervention scenarios, the results are displayed in Figure 5, with the sample size fixed at $n_e = 10000$ for each $e \in \mathcal{E}$. For NegDRO and DRIG, we evaluate the distance of the fitted estimators to the causal effect, as the regularization parameter γ varies in the range $[0, 60]$. Since CausalDantzig does not include a regularization parameter, its performance remains unchanged across different γ values. The figure shows that under the limited and weak intervention scenarios, DRIG estimators deviate from β^* as γ increases. Similarly, CausalDantzig fails to approximate β^* in these two scenarios. Only in the strong intervention setting, both CausalDantzig and DRIG (with a relatively large γ) achieve accurate approximation of β^* . In contrast, our proposed NegDRO consistently delivers estimators close to β^* across all three intervention settings as γ grows.

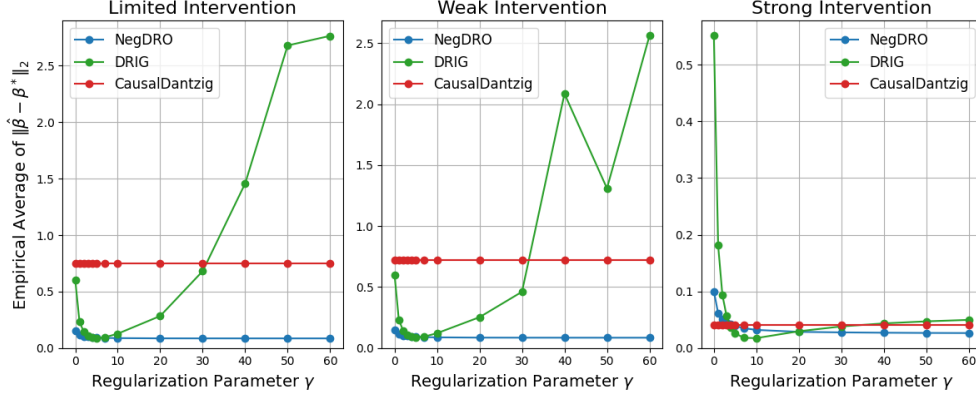


Figure 5: Comparison of NegDRO with CausalDantzig and DRIG in terms of estimators' ℓ_2 distance to the causal effect β^* , within three intervention scenarios as described in Example 2 in Section 5.2 with sample size $n_e = 10000$ for $e \in \mathcal{E}$. For NegDRO and DRIG, we vary the regularization parameter γ in the range of $[0, 60]$, while CausalDantzig does not require it. The results are averaged over 200 simulations.

6 Numerical Results

In this section, we illustrate the performance of our proposed NegDRO through empirical simulations, where we use Algorithm 1 for implementation and present the full details in the Appendix. We introduce the data generating mechanism and depict the corresponding causal graph in Figure 6. The covariates $X^{(e)} \in \mathbb{R}^p$ and

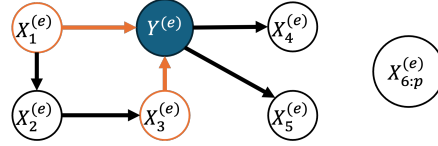


Figure 6: Illustration of (31): the highlighted covariates $X_1^{(e)}$ and $X_3^{(e)}$ are direct causes of $Y^{(e)}$.

the outcome $Y^{(e)} \in \mathbb{R}$ for each environment $e \in \mathcal{E} = \{1, 2, 3, 4\}$ are generated according to the following SEMs:

$$\begin{aligned} X_1^{(e)} &= \varepsilon_1^{(e)}, & X_2^{(e)} &= X_1^{(e)} + \varepsilon_2^{(e)}, & X_3^{(e)} &= X_2^{(e)} + \varepsilon_3^{(e)}, & Y^{(e)} &= X_1^{(e)} + X_3^{(e)} + \varepsilon_Y^{(e)}, \\ X_4^{(e)} &= Y^{(e)} + \varepsilon_4^{(e)}, & X_5^{(e)} &= -Y^{(e)} + \varepsilon_5^{(e)}, & X_{6:p}^{(e)} &= \varepsilon_{6:p}^{(e)}, \end{aligned} \quad (31)$$

where the noise terms $(\varepsilon_Y^{(e)}, \varepsilon_{1:p}^{(e)})^\top$ follow the error decomposition model (10) such that $(\varepsilon_Y^{(e)}, \varepsilon_{1:p}^{(e)})^\top = \eta + (0, \delta^{(e)})^\top$. Here, the systematic random error $\eta \sim \mathcal{N}(0_{p+1}, \mathbf{I}_{p+1})$ is shared across all environments, while the environment-specific interventions $\delta^{(e)} \in \mathbb{R}^p$ satisfy that $\delta_{6:p}^{(e)} \stackrel{iid}{\sim} \mathcal{N}(0, \frac{\varepsilon^2}{4})$ for all $e \in \mathcal{E}$, with

$$\delta_{1:5}^{(1)} = 0_5; \quad \delta_{1:5}^{(2)} \stackrel{iid}{\sim} \mathcal{N}(0, 9); \quad \delta_{1:5}^{(3)} = (1, 1.5, 2, 2.5, 3)^\top; \quad \delta_{1:5}^{(4)} \stackrel{iid}{\sim} \text{Unif}(-0.5, 0.5).$$

We simulate samples $\{x_i^{(e)}, y_i^{(e)}\}_{i=1}^{n_e}$ according to (31). For simplicity, the sample size is kept identical across all environments, with $n_e = n$ for all $e \in \mathcal{E}$. In this setup, the causal set is $S^* = \{1, 3\}$ with the causal effect $\beta^* = (1, 0, 1, 0_{p-3})^\top$.

Figure 7 illustrates the dependence of $\|\hat{b}^\gamma - \beta^*\|_2$, on the regularization parameter γ and the sample size n . The covariate dimension p is varied across $\{5, 20, 50\}$. On the left panel, the sample size is fixed

at $n = 20000$, while γ is varied within the range $[0, 25]$. The results show that as γ increases, the distance $\|\hat{b}^\gamma - \beta^*\|_2$ decreases similarly to the curve of $\frac{0.09}{1+4\gamma} + 0.05$, validating our Theorem 5 in terms of the dependence on γ . On the right panel, we examine the dependence of $\|\hat{b}^\gamma - \beta^*\|_2$ on the sample size n . We fix the regularization parameter as $\gamma = 20$, while varying n in the range of $[500, 20000]$. A benchmark curve $0.8n^{-1/4}$ is included for comparison. The logarithm-transformed distance $\log \|\hat{b}^\gamma - \beta^*\|_2$ decreases approximately at a rate of $-1/4 \cdot \log n + c$ for a positive constant $c > 0$, validating our Theorem 5 in terms of the dependence on the sample size.

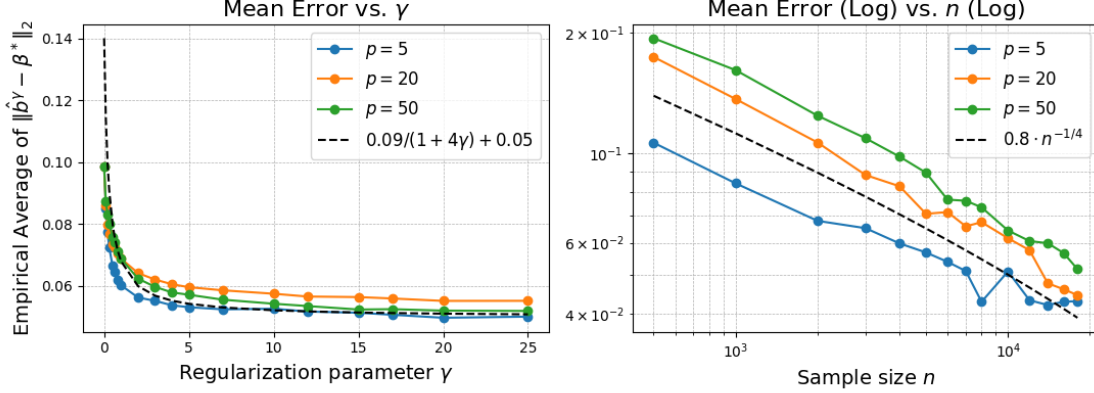


Figure 7: Dependence of $\|\hat{b}^\gamma - \beta^*\|_2$ on the regularization parameter γ and the sample size n , where \hat{b}^γ is the output of Algorithm 1. The dimension p is varied in $\{5, 20, 50\}$. On the left panel, the sample size is fixed at $n = 20000$, and the regularization parameter γ is varied within $[0, 25]$. On the right panel, The logarithm-transformed distance $\log \|\hat{b}^\gamma - \beta^*\|_2$ is plotted against $\log n$. Results are averaged over 200 simulations.

Next, we investigate the intervention scenarios by setting $\delta_{\delta;p}^{(e)} = 0_{p-5}$ for all $e \in \mathcal{E}$ within the SEMs in (31). We compare our NegDRO with other causal invariance learning methods in terms of both estimation accuracy (measured as the ℓ_2 distance to the causal effect β^*) and computational cost (measured in seconds). The methods included in the comparison are ICP [Peters et al., 2016], CausalDantzig [Meinshausen, 2018], DRIG [Shen et al., 2023], and EILLS [Fan et al., 2023]. The ERM method is also included for comparative purposes, which pools all observed data across environments and fits a least-squares model. We set the regularization parameter $\gamma = 20$ for our NegDRO. For EILLS, the hyperparameter is also set as $\gamma = 20$, following the recommendation in their original work. For other causal invariance learning approaches, their hyperparameters (if applicable) are chosen in an oracle manner: we enumerate a wide range of hyperparameter values and select the best one that minimizes ℓ_2 distance to β^* . Detailed implementations for all methods are provided in the Appendix.

The results are summarized in Figure 8, where we fix the sample size at $n = 5000$ and vary the dimension p in the range of $[5, 120]$. To ensure timely execution, we impose a 30-minute time limit for each method; if a method does not finish within this limit, it is terminated automatically. In the left panel of Figure 8, among the evaluated methods, only our NegDRO closely approximates β^* , irrespective of the covariate dimension p . Notably, EILLS performs exceptionally well in recovering the causal effect β^* , yielding a smaller ℓ_2 distance compared to all other methods for lower-dimensional settings when $p \in \{5, 10, 15, 20\}$. However, its computational time reaches the 30-minute time limit when $p \geq 25$, indicating the hardness of scaling up such integer programming algorithms for causal discovery. The ICP method, which prioritizes selecting direct causes through hypothesis testing rather than achieving accurate estimation of the causal effect, demonstrates conservative behavior in this setting, resulting in poor accuracy for estimating β^* . DRIG

and Causal Dantzig perform well when $p = 5$, but fail to approximate β^* for $p > 5$. This failure arises because their underlying assumptions are violated in our setting, where certain covariates remain unintervened, specifically with $\delta_{6;p}^{(e)} = 0_{p-5}$ for $e \in \mathcal{E}$; see detailed discussions in Section 5.2.

The right panel of Figure 8 tracks the computational time for each method. It is evident that ICP and EILLS, both of which rely on exhaustive search, quickly exceed the time limit as the covariate dimension p increases, specifically at $p = 20$ and $p = 25$, respectively. In contrast, all other methods, including our proposed NegDRO, demonstrate computational costs that scale polynomially with the dimension p .

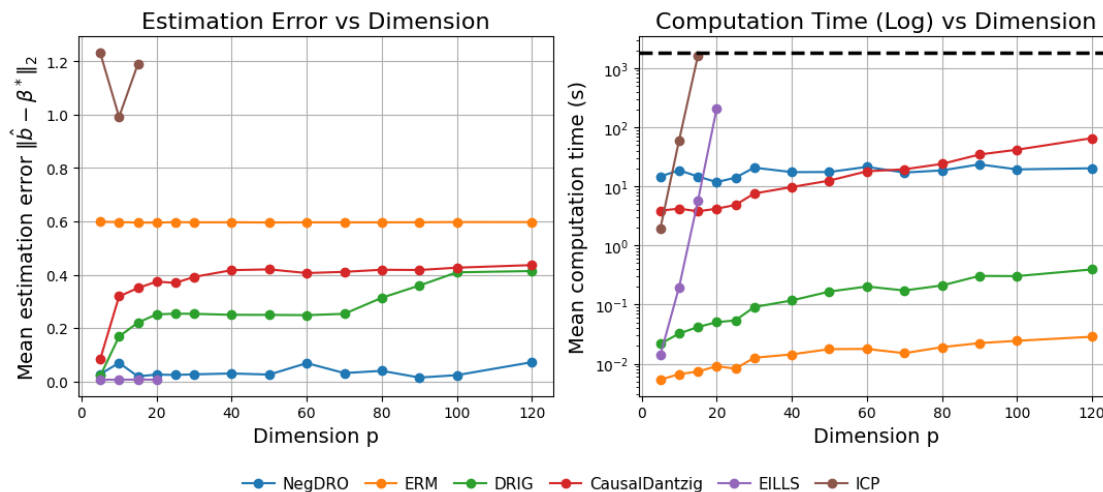


Figure 8: Comparison of different causal invariance learning methods in terms of the estimation accuracy and computational time. The covariate dimension p varies within the range of $[5, 120]$, while the sample size is fixed at $n_e = 5,000$ for each $e \in \mathcal{E}$. The left panel displays the ℓ_2 distance between each method’s estimator and the causal effect β^* . The right panel depicts the computational cost (logarithm of seconds) for each method, with a black dashed horizontal line marking the 30-minute time limit. Methods exceeding this limit are terminated. Results are averaged over 200 simulations.

Acknowledgement

The authors extend their gratitude to Nicolai Meinshausen and Yihong Gu for their valuable discussions and insights. The research of Z. Wang and Z. Guo was partly supported by the NSF grant DMS 2015373 and NIH grants R01GM140463 and R01LM013614. Z. Guo also acknowledges financial support for visiting the Institute of Mathematical Research (FIM) at ETH Zurich. Y. Hu was supported by NCCR Automation, a National Centre of Competence in Research, funded by the Swiss National Science Foundation (grant number 51NF40_225155).

References

- J. Aldrich. Autonomy. *Oxford Economic Papers*, 41(1):15–34, 1989. (Cited on page 8.)
- S. A. Andersson, D. Madigan, and M. D. Perlman. A characterization of markov equivalence classes for acyclic digraphs. *The Annals of Statistics*, 25(2):505–541, 1997. (Cited on page 5.)
- M. Arjovsky, L. Bottou, I. Gulrajani, and D. Lopez-Paz. Invariant risk minimization. *arXiv preprint arXiv:1907.02893*, 2019. (Cited on pages 2, 4, and 5.)

- A. Auslender and M. Teboulle. Projected subgradient methods with non-euclidean distances for non-differentiable convex minimization and variational inequalities. *Mathematical Programming*, 120:27–48, 2009. (Cited on page 11.)
- K. Baicker, S. L. Taubman, H. L. Allen, M. Bernstein, J. H. Gruber, J. P. Newhouse, E. C. Schneider, B. J. Wright, A. M. Zaslavsky, and A. N. Finkelstein. The oregon experiment—effects of medicaid on clinical outcomes. *New England Journal of Medicine*, 368(18):1713–1722, 2013. (Cited on page 1.)
- A. V. Banerjee and E. Duflo. The experimental approach to development economics. *Annu. Rev. Econ.*, 1(1):151–178, 2009. (Cited on page 22.)
- S. Beery, G. Van Horn, and P. Perona. Recognition in terra incognita. In *Proceedings of the European conference on computer vision (ECCV)*, pages 456–473, 2018. (Cited on page 2.)
- A. Ben-Tal and M. Teboulle. Hidden convexity in some nonconvex quadratically constrained quadratic programming. *Mathematical Programming*, 72(1):51–63, 1996. (Cited on page 5.)
- A. Ben-Tal, D. Den Hertog, A. De Waegenaere, B. Melenberg, and G. Rennen. Robust solutions of optimization problems affected by uncertain probabilities. *Management Science*, 59(2):341–357, 2013. (Cited on page 9.)
- D. P. Bertsekas. Nonlinear programming. *Journal of the Operational Research Society*, 48(3):334–334, 1997. (Cited on page 16.)
- K. A. Bollen. *Structural equations with latent variables*. John Wiley & Sons, 2014. (Cited on page 6.)
- J.-F. Bonnans, J. C. Gilbert, C. Lemaréchal, and C. A. Sagastizábal. *Numerical optimization: theoretical and practical aspects*. Springer Science & Business Media, 2006. (Cited on pages 10 and 16.)
- L. Bottou, F. E. Curtis, and J. Nocedal. Optimization methods for large-scale machine learning. *SIAM review*, 60(2):223–311, 2018. (Cited on page 19.)
- S. Boyd and L. Vandenberghe. *Convex optimization*. Cambridge university press, 2004. (Cited on pages 10 and 16.)
- W. Brannath, E. Zuber, M. Branson, F. Bretz, P. Gallo, M. Posch, and A. Racine-Poon. Confirmatory adaptive designs with bayesian decision tools for a targeted therapy in oncology. *Statistics in medicine*, 28(10):1445–1463, 2009. (Cited on page 22.)
- Y. Carmon, J. C. Duchi, O. Hinder, and A. Sidford. Lower bounds for finding stationary points i. *Mathematical Programming*, 184(1):71–120, 2020. (Cited on page 19.)
- G. H. Chen and R. T. Rockafellar. Convergence rates in forward–backward splitting. *SIAM Journal on Optimization*, 7(2):421–444, 1997. (Cited on page 11.)
- X. Chen, N. He, Y. Hu, and Z. Ye. Efficient algorithms for a class of stochastic hidden convex optimization and its applications in network revenue management. *Operations Research*, 2024a. (Cited on page 5.)
- X. Chen, Y. Hu, and M. Zhao. Landscape of policy optimization for finite horizon mdps with general state and action. *arXiv preprint arXiv:2409.17138*, 2024b. (Cited on page 5.)
- D. M. Chickering. Optimal structure identification with greedy search. *Journal of machine learning research*, 3(Nov):507–554, 2002. (Cited on page 5.)

- C.-Y. Chuang, A. Torralba, and S. Jegelka. Estimating generalization under distribution shifts via domain-invariant representations. *arXiv preprint arXiv:2007.03511*, 2020. (Cited on page 5.)
- O. Cohen, N. D. Rubinstein, A. Stern, U. Gophna, and T. Pupko. A likelihood framework to analyse phyletic patterns. *Philosophical Transactions of the Royal Society B: Biological Sciences*, 363(1512):3903–3911, 2008. (Cited on page 22.)
- P. Daniusis, D. Janzing, J. Mooij, J. Zscheischler, B. Steudel, K. Zhang, and B. Schölkopf. Inferring deterministic causal relations. *arXiv preprint arXiv:1203.3475*, 2012. (Cited on page 11.)
- J. M. Danskin. The theory of max-min, with applications. *SIAM Journal on Applied Mathematics*, 14(4):641–664, 1966. (Cited on page 16.)
- Y. N. Dauphin, R. Pascanu, C. Gulcehre, K. Cho, S. Ganguli, and Y. Bengio. Identifying and attacking the saddle point problem in high-dimensional non-convex optimization. *Advances in neural information processing systems*, 27, 2014. (Cited on page 16.)
- D. Davis and D. Drusvyatskiy. Complexity of finding near-stationary points of convex functions stochastically. *arXiv preprint arXiv:1802.08556*, 2018. (Cited on page 22.)
- A. Dawid and V. Didelez. Identifying the consequences of dynamic treatment strategies: A decision theoretic overview. *Statistics Surveys*, 4:184–231, 2010. (Cited on page 8.)
- E. Duffo, R. Glennerster, and M. Kremer. Using randomization in development economics research: A toolkit. *Handbook of development economics*, 4:3895–3962, 2007. (Cited on page 1.)
- F. Eberhardt, N. Kaynar, and A. Siddiq. Discovering causal models with optimization: Confounders, cycles, and instrument validity. *Management Science*, 2024. (Cited on page 5.)
- J. Fan, C. Fang, Y. Gu, and T. Zhang. Environment invariant linear least squares. *arXiv preprint arXiv:2303.03092*, 2023. (Cited on pages 2, 3, 4, 8, 9, 14, 18, and 28.)
- M. H. Farrell, T. Liang, and S. Misra. Deep neural networks for estimation and inference: application to causal effects and other semiparametric estimands. *arXiv preprint arXiv:1809.09953*, 20, 2018. (Cited on page 1.)
- I. Fatkhullin, J. Etesami, N. He, and N. Kiyavash. Sharp analysis of stochastic optimization under global kurdyka-{\mathcal{L}} ojasiewicz inequality. *arXiv preprint arXiv:2210.01748*, 2022. (Cited on page 5.)
- I. Fatkhullin, N. He, and Y. Hu. Stochastic optimization under hidden convexity. *arXiv preprint arXiv:2401.00108*, 2023. (Cited on page 5.)
- Q. Feng and J. G. Shanthikumar. Supply and demand functions in inventory models. *Operations Research*, 66(1):77–91, 2018. (Cited on page 5.)
- S. Ghadimi and G. Lan. Stochastic first-and zeroth-order methods for nonconvex stochastic programming. *SIAM journal on optimization*, 23(4):2341–2368, 2013. (Cited on page 18.)
- A. Ghassami, S. Salehkaleybar, N. Kiyavash, and K. Zhang. Learning causal structures using regression invariance. *Advances in Neural Information Processing Systems*, 30, 2017. (Cited on pages 2, 3, 4, 8, 9, 11, 12, and 23.)
- Z. Guo. Statistical inference for maximin effects: Identifying stable associations across multiple studies. *Journal of the American Statistical Association*, 119(547):1968–1984, 2024. (Cited on page 5.)

- T. Haavelmo. The probability approach in econometrics. *Econometrica: Journal of the Econometric Society*, pages iii–115, 1944. (Cited on page 8.)
- T. Hashimoto, M. Srivastava, H. Namkoong, and P. Liang. Fairness without demographics in repeated loss minimization. In *International Conference on Machine Learning*, pages 1929–1938. PMLR, 2018. (Cited on page 10.)
- A. Hauser and P. Bühlmann. Characterization and greedy learning of interventional markov equivalence classes of directed acyclic graphs. *The Journal of Machine Learning Research*, 13(1):2409–2464, 2012. (Cited on page 5.)
- A. Hauser and P. Bühlmann. Jointly interventional and observational data: estimation of interventional markov equivalence classes of directed acyclic graphs. *Journal of the Royal Statistical Society Series B: Statistical Methodology*, 77(1):291–318, 2015. (Cited on pages 3, 5, and 23.)
- Y.-B. He and Z. Geng. Active learning of causal networks with intervention experiments and optimal designs. *Journal of Machine Learning Research*, 9(Nov):2523–2547, 2008. (Cited on page 3.)
- C. Heinze-Deml, J. Peters, and N. Meinshausen. Invariant causal prediction for nonlinear models. *Journal of Causal Inference*, 6(2):20170016, 2018. (Cited on page 9.)
- M. Heusel, H. Ramsauer, T. Unterthiner, B. Nessler, and S. Hochreiter. Gans trained by a two time-scale update rule converge to a local nash equilibrium. *Advances in neural information processing systems*, 30, 2017. (Cited on page 11.)
- P. Hoyer, D. Janzing, J. M. Mooij, J. Peters, and B. Schölkopf. Nonlinear causal discovery with additive noise models. *Advances in neural information processing systems*, 21, 2008. (Cited on page 11.)
- G. W. Imbens and D. B. Rubin. *Causal inference in statistics, social, and biomedical sciences*. Cambridge university press, 2015. (Cited on page 7.)
- D. Janzing and B. Schölkopf. Causal inference using the algorithmic markov condition. *IEEE Transactions on Information Theory*, 56(10):5168–5194, 2010. (Cited on page 11.)
- D. Janzing, J. Mooij, K. Zhang, J. Lemeire, J. Zscheischler, P. Daniušis, B. Steudel, and B. Schölkopf. Information-geometric approach to inferring causal directions. *Artificial Intelligence*, 182:1–31, 2012. (Cited on page 11.)
- M. Kalisch and P. Bühlman. Estimating high-dimensional directed acyclic graphs with the pc-algorithm. *Journal of Machine Learning Research*, 8(3), 2007. (Cited on page 5.)
- P. Kamath, A. Tangella, D. Sutherland, and N. Srebro. Does invariant risk minimization capture invariance? In *International Conference on Artificial Intelligence and Statistics*, pages 4069–4077. PMLR, 2021. (Cited on page 5.)
- H. Karimi, J. Nutini, and M. Schmidt. Linear convergence of gradient and proximal-gradient methods under the polyak-łojasiewicz condition. In *Joint European conference on machine learning and knowledge discovery in databases*, pages 795–811. Springer, 2016. (Cited on pages 5 and 20.)
- D. P. Kingma. Adam: A method for stochastic optimization. *arXiv preprint arXiv:1412.6980*, 2014. (Cited on page 18.)
- S. Klein, S. Weissmann, and L. Döring. Beyond stationarity: Convergence analysis of stochastic softmax policy gradient methods. *arXiv preprint arXiv:2310.02671*, 2023. (Cited on page 5.)

- G. M. Korpelevich. The extragradient method for finding saddle points and other problems. *Matecon*, 12: 747–756, 1976. (Cited on page 11.)
- D. Krueger, E. Caballero, J.-H. Jacobsen, A. Zhang, J. Binas, D. Zhang, R. Le Priol, and A. Courville. Out-of-distribution generalization via risk extrapolation (rex). In *International conference on machine learning*, pages 5815–5826. PMLR, 2021. (Cited on page 5.)
- K. Kurdyka. On gradients of functions definable in o-minimal structures. In *Annales de l’institut Fourier*, volume 48, pages 769–783, 1998. (Cited on page 5.)
- G. Lan. Policy mirror descent for reinforcement learning: Linear convergence, new sampling complexity, and generalized problem classes. *Mathematical programming*, 198(1):1059–1106, 2023. (Cited on page 5.)
- J. D. Lee, M. Simchowitz, M. I. Jordan, and B. Recht. Gradient descent only converges to minimizers. In *Conference on learning theory*, pages 1246–1257. PMLR, 2016. (Cited on page 18.)
- T. Lin, C. Jin, and M. I. Jordan. Near-optimal algorithms for minimax optimization. In *Conference on Learning Theory*, pages 2738–2779. PMLR, 2020. (Cited on page 11.)
- T. Lin, C. Jin, M. Jordan, et al. Two-timescale gradient descent ascent algorithms for nonconvex minimax optimization. *arXiv preprint arXiv:2408.11974*, 2024. (Cited on page 11.)
- J. Liu, Z. Hu, P. Cui, B. Li, and Z. Shen. Heterogeneous risk minimization. In *International Conference on Machine Learning*, pages 6804–6814. PMLR, 2021. (Cited on page 5.)
- S. Lojasiewicz. A topological property of real analytic subsets. *Coll. du CNRS, Les équations aux dérivées partielles*, 117(87-89):2, 1963. (Cited on page 5.)
- C. Lu, Y. Wu, J. M. Hernández-Lobato, and B. Schölkopf. Nonlinear invariant risk minimization: A causal approach. *arXiv preprint arXiv:2102.12353*, 2021. (Cited on page 5.)
- J. Ludwig, G. J. Duncan, L. A. Gennetian, L. F. Katz, R. C. Kessler, J. R. Kling, and L. Sanbonmatsu. Long-term neighborhood effects on low-income families: Evidence from moving to opportunity. *American economic review*, 103(3):226–231, 2013. (Cited on page 1.)
- S. Magliacane, T. Van Ommen, T. Claassen, S. Bongers, P. Versteeg, and J. M. Mooij. Domain adaptation by using causal inference to predict invariant conditional distributions. *Advances in neural information processing systems*, 31, 2018. (Cited on page 2.)
- N. Meinshausen. Causality from a distributional robustness point of view. In *2018 IEEE Data Science Workshop (DSW)*, pages 6–10. IEEE, 2018. (Cited on page 28.)
- N. Meinshausen and P. Bühlmann. Maximin effects in inhomogeneous large-scale data. 2015. (Cited on page 5.)
- N. Meinshausen, A. Hauser, J. M. Mooij, J. Peters, P. Versteeg, and P. Bühlmann. Methods for causal inference from gene perturbation experiments and validation. *Proceedings of the National Academy of Sciences*, 113(27):7361–7368, 2016. (Cited on page 2.)
- S. Morgan. *Counterfactuals and causal inference*. Cambridge University Press, 2015. (Cited on page 7.)
- H. Namkoong and J. C. Duchi. Stochastic gradient methods for distributionally robust optimization with f-divergences. *Advances in neural information processing systems*, 29, 2016. (Cited on page 9.)

- A. Nedić and A. Ozdaglar. Subgradient methods for saddle-point problems. *Journal of optimization theory and applications*, 142:205–228, 2009. (Cited on page 11.)
- A. Nemirovski. Prox-method with rate of convergence $o(1/t)$ for variational inequalities with lipschitz continuous monotone operators and smooth convex-concave saddle point problems. *SIAM Journal on Optimization*, 15(1):229–251, 2004. (Cited on page 11.)
- Y. Nesterov et al. *Lectures on convex optimization*, volume 137. Springer, 2018. (Cited on page 19.)
- B. Nye, L. V. Hedges, and S. Konstantopoulos. The effects of small classes on academic achievement: The results of the tennessee class size experiment. *American Educational Research Journal*, 37(1):123–151, 2000. (Cited on page 1.)
- J. Pearl. *Causality*. Cambridge university press, 2009. (Cited on pages 6 and 13.)
- J. Pearl, M. Glymour, and N. P. Jewell. *Causal inference in statistics: A primer*. John Wiley & Sons, 2016. (Cited on page 6.)
- J. Peters, J. M. Mooij, D. Janzing, and B. Schölkopf. Causal discovery with continuous additive noise models. 2014. (Cited on pages 11 and 12.)
- J. Peters, P. Bühlmann, and N. Meinshausen. Causal inference by using invariant prediction: identification and confidence intervals. *Journal of the Royal Statistical Society Series B: Statistical Methodology*, 78(5):947–1012, 2016. (Cited on pages 2, 3, 4, 8, 9, 23, and 28.)
- N. Pfister, P. Bühlmann, and J. Peters. Invariant causal prediction for sequential data. *Journal of the American Statistical Association*, 114(527):1264–1276, 2019. (Cited on pages 2 and 9.)
- N. Pfister, E. G. Williams, J. Peters, R. Aebbersold, and P. Bühlmann. Stabilizing variable selection and regression. *The Annals of Applied Statistics*, 15(3):1220–1246, 2021. (Cited on pages 2 and 8.)
- A. Polinelli, V. Vinciotti, and E. C. Wit. Generalised causal dantzig. *arXiv preprint arXiv:2407.16786*, 2024. (Cited on page 11.)
- B. T. Polyak et al. Gradient methods for minimizing functionals. *Zhurnal vychislitel’noi matematiki i matematicheskoi fiziki*, 3(4):643–653, 1963. (Cited on page 5.)
- H. Rafique, M. Liu, Q. Lin, and T. Yang. Weakly-convex–concave min–max optimization: provable algorithms and applications in machine learning. *Optimization Methods and Software*, 37(3):1087–1121, 2022. (Cited on page 11.)
- H. Rahimian and S. Mehrotra. Frameworks and results in distributionally robust optimization. *Open Journal of Mathematical Optimization*, 3:1–85, 2022. (Cited on page 11.)
- M. Rojas-Carulla, B. Schölkopf, R. Turner, and J. Peters. Invariant models for causal transfer learning. *Journal of Machine Learning Research*, 19(36):1–34, 2018. (Cited on pages 2, 4, 8, and 9.)
- E. Rosenfeld, P. Ravikumar, and A. Risteski. The risks of invariant risk minimization. *arXiv preprint arXiv:2010.05761*, 2020. (Cited on page 5.)
- D. Rothenhäusler, P. Bühlmann, and N. Meinshausen. Causal dantzig. *The Annals of Statistics*, 47(3):1688–1722, 2019. (Cited on pages 3, 4, 8, 11, 12, 13, 18, 23, and 25.)

- D. Rothenhäusler, N. Meinshausen, P. Bühlmann, and J. Peters. Anchor regression: Heterogeneous data meet causality. *Journal of the Royal Statistical Society Series B: Statistical Methodology*, 83(2):215–246, 2021. (Cited on pages 3, 11, and 12.)
- S. Sagawa, P. W. Koh, T. B. Hashimoto, and P. Liang. Distributionally robust neural networks for group shifts: On the importance of regularization for worst-case generalization. *arXiv preprint arXiv:1911.08731*, 2019. (Cited on pages 4, 5, and 10.)
- B. Schölkopf. Causality for machine learning. In *Probabilistic and causal inference: The works of Judea Pearl*, pages 765–804. 2022. (Cited on page 1.)
- B. Schölkopf, F. Locatello, S. Bauer, N. R. Ke, N. Kalchbrenner, A. Goyal, and Y. Bengio. Toward causal representation learning. *Proceedings of the IEEE*, 109(5):612–634, 2021. (Cited on page 1.)
- A. Sharma and E. Kiciman. Dowhy: An end-to-end library for causal inference. *arXiv preprint arXiv:2011.04216*, 2020. (Cited on page 1.)
- X. Shen, P. Bühlmann, and A. Taeb. Causality-oriented robustness: exploiting general additive interventions. *arXiv preprint arXiv:2307.10299*, 2023. (Cited on pages 3, 4, 11, 12, 23, 25, and 28.)
- P. Spirtes, C. Glymour, and R. Scheines. *Causation, prediction, and search*. MIT press, 2001. (Cited on pages 6 and 13.)
- J. Sun. Provable nonconvex methods/algorithms. 2021. URL <https://sunju.org/research/nonconvex/>. (Cited on page 5.)
- A. Taeb, J. L. Gamella, C. Heinze-Deml, and P. Bühlmann. Learning and scoring gaussian latent variable causal models with unknown additive interventions. *Journal of Machine Learning Research*, 25(293): 1–68, 2024. (Cited on page 5.)
- T. Verma and J. Pearl. Equivalence and synthesis of causal models. In *Proceedings of the Sixth Annual Conference on Uncertainty in Artificial Intelligence*, pages 255–270, 1990. (Cited on page 5.)
- R. Wang, M. Yi, Z. Chen, and S. Zhu. Out-of-distribution generalization with causal invariant transformations. In *Proceedings of the IEEE/CVF Conference on Computer Vision and Pattern Recognition*, pages 375–385, 2022. (Cited on page 2.)
- Z. Wang, P. Bühlmann, and Z. Guo. Distributionally robust machine learning with multi-source data. *arXiv preprint arXiv:2309.02211*, 2023. (Cited on page 5.)
- J. M. Wooldridge. *Introductory Econometrics: A Modern Approach*. ISE - International Student Edition. South-Western, 2009. ISBN 9780324581621. URL <http://books.google.ch/books?id=64vt5TDBNLwC>. (Cited on page 7.)
- M. Yin, Y. Wang, and D. M. Blei. Optimization-based causal estimation from heterogeneous environments. *Journal of Machine Learning Research*, 25:1–44, 2024. (Cited on pages 3, 8, and 14.)